Current Sensing Techniques: A Review

Silvio Ziegler, Robert C. Woodward, Herbert Ho-Ching Iu, *Senior Member, IEEE*, and Lawrence J. Borle, *Member, IEEE*

***Abstract*—This paper provides a thorough review of state-of-the-art current sensing techniques. It catalogues the current sensors according to the underlying physical principle in order to point out their strengths and weaknesses.**

New current sensing principles based on either established techniques such as Hall-effect sensors and fluxgate principles or emerging technologies such as magneto resistance effect and fiber-optical techniques provide attractive alternatives for current sensing, although generally at a higher price than traditional techniques like shunt resistors.

***Index Terms*—Current measurement, current transformers, fluxgates, Hall-effect sensors, magnetoresistance, shunt resistor.**

I. Introduction

INFORMATION regarding current flow is required in a wide range of electrical and electronics applications. Each application has different performance requirements in terms of cost, isolation, precision, bandwidth, measurement range, or size and many different current measurement methods have been developed to satisfy these demands. Today, current information increasingly needs to be available in digital form for digital control or monitoring purposes. This requires the output signal of a particular current sensing technique to be acquired by an analog-to-digital converter.

As an example, shunt resistors have been used extensively in power electronics due to their low cost, small size, and relative simplicity, while providing reasonable accuracy. To achieve higher integration, higher efficiency and enable more sophisticated control techniques, the analog control loops are increasingly replaced by digital control loops. Accordingly, the current information needs to be digitalized. The small voltage drop across a shunt resistor needs amplification, which alters the bandwidth, and increases the device size and cost. Power converters, moreover, have reached a power density level, where the power losses inside shunt resistor start to become troublesome. Therefore, power electronics engineers are seeking alternatives for shunt resistors with similar accuracy but lower power losses, and with an output voltage that can be directly sampled by an analog-to-digital converter.

Manuscript received September 20, 2008; accepted October 27, 2008. Current version published February 27, 2009. This work was supported in part by the company Power-One, Inc. The associate editor coordinating the review of this paper and approving it for publication was Dr. Kailash Thakur.

S. Ziegler, H. H. C. Iu, and L. J. Borle are with the School of Electrical, Electronic and Computer Engineering, University of Western Australia, Crawley, WA 6009, Australia (e-mail: silvio.ziegler@gemhelp.ch; herbert@ee.uwa.edu.au; lborle@ee.uwa.edu.au).

R. C. Woodward is with the School of Physics, University of Western Australia, Crawley, WA 6009, Australia (e-mail: woodward@physics.uwa.edu.au).

Color versions of one or more of the figures in this paper are available online at http://ieeexplore.ieee.org.

Digital Object Identifier 10.1109/JSEN.2009.2013914

The aim of this paper is to provide the reader with a fundamental understanding of the techniques available for current monitoring and some understanding of the performance and limitations of each technique. Therefore, we have classified the current sensing techniques based upon the underlying fundamental physical principle. These principles are the following.

1) Ohm's law of resistance.
2) Faraday's law of induction.
3) Magnetic field sensors.
4) Faraday effect.

In addition, we will discuss known sensing configuration, such as open-loop, closed-loop, with particular reference to magnetic field sensors, and the use of combinations of sensors in order to meet more demanding performance requirements.

II. Current Sensors Based Upon Ohm's Law of Resistance

Ohm's law of resistance is basically a simplification of the Lorentz law that states

$$\mathbf{J} = \sigma(\mathbf{E} + \mathbf{v} \times \mathbf{B}). \tag{1}$$

$\mathbf{J}$ is the current density, $\mathbf{E}$ the electric field, $\mathbf{v}$ the charge velocity, $\mathbf{B}$ the magnetic flux density acting onto the charge, and σ the material conductivity. In most cases, the velocity of the moving charges is sufficiently small that the second term can be neglected

$$\mathbf{J} = \sigma\mathbf{E}. \tag{2}$$

This equation is known as Ohm's law of resistance and states that the voltage drop across a resistor is proportional to the flowing current. This simple relationship can be exploited to sense currents. These current sensors often provide the advantage of lower costs compared with other sensing techniques, and have the reputation of being reliable due to their simple working principle.

A. Shunt Resistor

A common approach due to its simplicity is the use of a shunt resistor for current sensing. The voltage drop across the shunt resistor is used as a proportional measure of the current flow. It can be used to sense both alternating currents (AC) and direct currents (DC). The shunt resistor is introduced into the current conducting path, and can, therefore, generate a substantial amount of power loss. The power loss can be calculated via Ohm's law (i^2R) and increases with the square of the current. This power loss may restrict the use of shunt resistors in high current applications.

1) High-Performance Coaxial Shunt: Shunt resistors have been used extensively to measure transient current pulses with fast rise-times and high amplitudes. In such applications, the

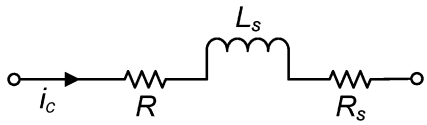

Fig. 1. Equivalent circuit diagram for a shunt resistor.

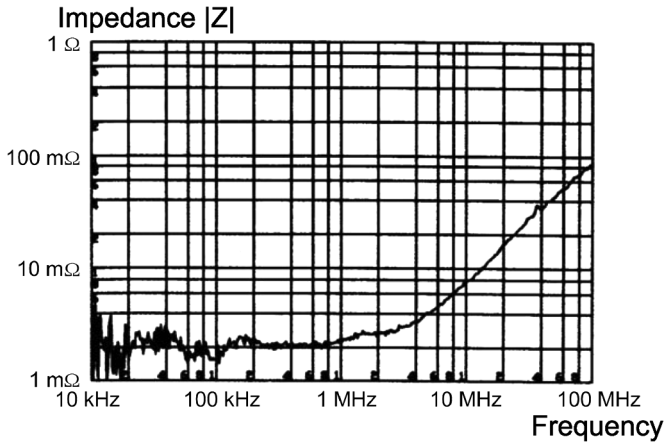

Fig. 2. Impedance measurement of a typical SMD shunt resistor (WSL2512, 3 mΩ – image courtesy of Vishay Dale, Inc.).

high-frequency behavior of the shunt resistor is of critical importance. Fig. 1 shows the equivalent circuit diagram of a shunt resistor with a nominal resistance R, including a parasitic inductance L_s and the series resistance R_s due to skin effect. The parasitic inductance L_s is often a source of confusion since it is frequently assumed to be related to the self-inductance of the shunt resistor. In reality, the parasitic inductance is determined by the mutual inductance M between loop built by the sense wires and the loop built by the main current [1]. Hence, the connection of the sense wires is crucial to achieve good performance. Significant research has been conducted to reduce L_s in order to increase the measurement bandwidth. Geometrical embodiments, e.g., coaxial resistive tube, have been found, which significantly reduce the parasitic inductance by reducing the flux that couples into the sense wires [2]–[4]. For coaxial shunt resistors, the skin effect is notable since the parasitic inductance is very small due to the superior coaxial construction. For heavy duty shunts that measure pulse currents with magnitudes of 100 kA, the skin effect can become the limiting factor that determines the measurement bandwidth [5]. Ironically, it has been found that by ensuring that a certain amount of flux couples into the measurement wire the skin effect can be compensated by the induced voltage [4], [5]. Another technique uses a flat strap geometry [6]. These methods allow the measurement of current pulses with rise times of a few nanoseconds and magnitudes of several kA.

2) Low-Cost Surface-Mounted-Device (SMD): For highly integrated electronic devices, coaxial shunt resistors are not suitable since they are bulky and expensive, and their usefulness is generally limited to the measurement of fast current pulses. In the majority of cases, thick film structures are used that can be integrated into surface-mounted-devices (SMDs) [7]. These shunt resistors are commonly used to sense direct currents up to 100–200 A. For higher current levels, the losses become substantial, which results in bulky shunt resistors that may not be suitable for device integration. Unfortunately, the higher integration comes at the cost of substantial higher parasitic inductance compared with optimized heavy-duty shunt resistors. Due to the small physical dimensions of SMD resistors, the skin effect becomes secondary, and a first-order model incorporates only the ohmic resistance R and the parasitic inductance L_s. The accurateness of this model is verified in the impedance measurement in Fig. 2 of a typical SMD shunt resistor. It has to be noted that the frequency response will be deteriorated if the area enclosed by the sense wires is increased. Accordingly, it is important to understand how the manufacturer of the shunt resistor measured the parasitic inductance in order to predict the performance for the intended application. The resistor then shows a 20 dB/decade rise in the impedance value after the corner frequency is reached as predicted by the circuit model. The corner frequency f_c can be calculated according to

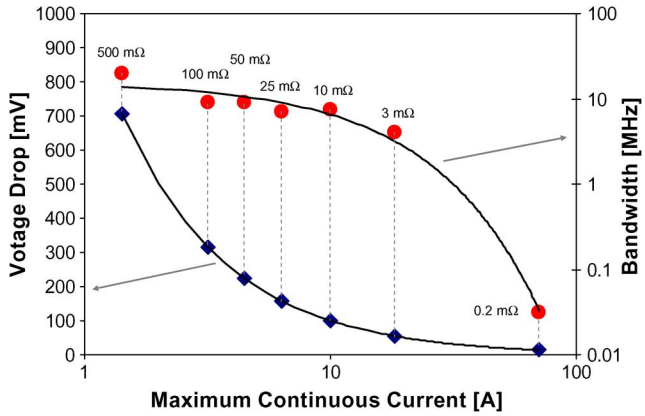

Fig. 3. Bandwidth and voltage drop of shunt resistors based on a series of exemplary SMD resistors at a power dissipation of 1 W.

$$f_c = \frac{R}{2\pi L_s}. \tag{3}$$

This formula is only valid if the skin effect is negligible small. In this case, it is feasible to improve the frequency response by employing a first-order low-pass filter [8]. The corner frequency is defined, where the reactance of the inductance is equal to the ohmic resistance. For this first-order system, the bandwidth is equal to the corner frequency. In Fig. 3, the bandwidth together with the voltage drop across the shunt resistor has been plotted against the current for a series of SMD resistors. The resistance values were chosen to maintain a constant power dissipation of one watt. The experimentally derived parasitic inductance data was obtained from the supplier Vishay Dale, Inc. (WSL 2512 Series), or for the 0.2 mΩ resistor (BVS-Z-R002) from Isabellenhuette GmbH. Fig. 3 demonstrates that measuring high currents with a shunt resistor leads to low bandwidth and low output voltages. Naturally, the lower the voltage drop the more gain is required to provide satisfactory output voltage for the analog-to-digital converter. As operational amplifiers have a constant gain-bandwidth-product this means that at high gains the bandwidth is further reduced. Depending on the design, either the amplifier or the shunt resistor will determine the maximum bandwidth of the measurement.

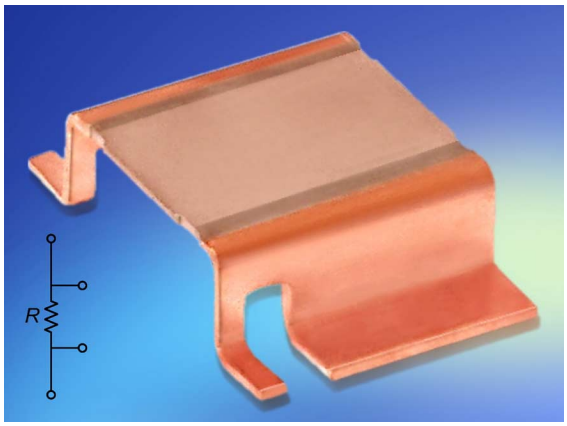

Fig. 4. A dedicated sense connection can overcome the problem with the high-temperature coefficient of the resistance at the soldering points (photo courtesy Isabellenhuette GmbH).

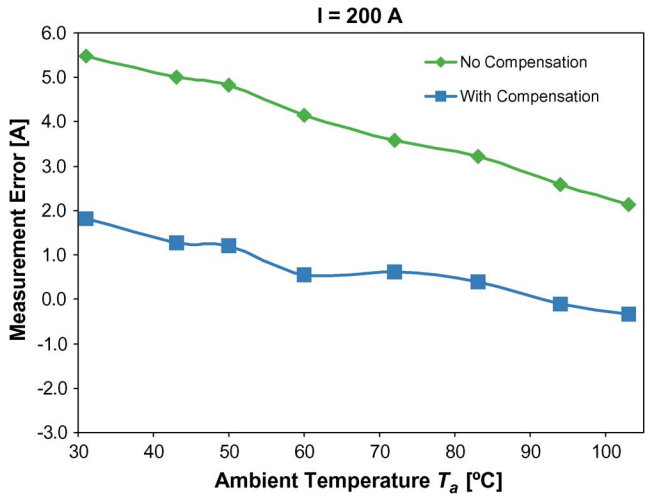

Fig. 5. Measurement of the absolute sensing error of the copper trace current sense method at a current of 200 A. The thermal resistance between the temperature sensor and copper trace leads to an underestimation of the temperature that can be corrected using a compensation technique [14].

An important characteristic of shunt resistors is their thermal drift. Shunt resistors are built with materials that exhibit a low temperature coefficient of resistivity like manganese-copper or nickel-chrome alloys [9]. With these alloys, manufacturers achieve very low values for the temperature coefficient of resistance (<20 ppm/K). Given the good thermal stability of the shunt resistor itself, the temperature coefficient of the contact resistance between the shunt resistor and the printed-circuit-board (PCB) can become the major source of error. Since the temperature coefficient of this resistance is high, it may contribute a considerable amount to the overall thermal drift of the device, even if the contact resistance itself is much lower than the shunt resistor value. The problem is exacerbated at very low shunt resistor values. To overcome this obstacle, sophisticated shunt resistors implement the four-wire Kelvin principle, which uses a dedicated sense connection (Fig. 4). Alternatively, the four-wire principle can be emulated using a conventional surface-mounted shunt resistor by connecting the sense wires on the inner side of the pads [9].

3) Application of Shunt Resistors: Shunt resistors can be inserted into either the forward or return current path. If the shunt is used in the return path, its voltage is relative to ground and can be amplified by a range of well-known techniques. In this configuration, the shunt resistor causes a voltage drop in the ground path, which means that circuits connected after the shunt resistor are not related to ground anymore. This can become a problem for some analog circuits. In addition, a fault condition inside the circuit monitored by the shunt resistor can lead to a current surge that bypasses the low-side shunt resistor (e.g., short circuit to ground). The ground path current measurement cannot detect such faults. A high-side current monitor is able to detect such incidents [10]. High-side current monitoring means that the shunt resistor is introduced into the forward current path and has a potential above ground. While this solves problems with uneven ground potentials, and undetected fault situations, it complicates the amplification stage since the voltage to be measured may be on a high-voltage potential. If this voltage potential is of practical amplitude, an integrated high-side current monitor or differential amplifier can be employed. Many semiconductor companies have high-side current monitors in their portfolios with some of them able to work with common-mode voltages from −16 up to 80 V with a bandwidth of around 1 MHz at a gain of 100.

High-performance coaxial shunt resistors are used to measure high impulse currents in specialized applications such as exploding wire circuits, nuclear fusion, and lightning studies. Surface mounted devices, on the other hand, are employed in power converter systems, industrial applications, mobile devices, and consumer electronics.

B. Trace Resistance Sensing

Instead of using a dedicated shunt resistor, it is possible to use the intrinsic resistance of a conducting element in the circuit (usually a copper trace or busbar). This approach promises very low-cost with no additional power losses. Naturally, the resistance of a copper trace is very low, and thus the resulting voltage drop is very small [11]. To get a useful output signal, an amplifier with high gain is required. The limited gain-bandwidth-product of the amplifier will then alter the performance of this current sensing method.

Spaziani [11] provided design equations and recommendations for a PCB copper shunt resistor. However, he concluded that this approach is not suitable for applications requiring reasonable accuracy due to the large thermal drift. Unlike a dedicated shunt resistor, copper exhibits strong thermal drift (the temperature coefficient of resistance for copper, Cu-ETP, is around 3930 ppm/K [12]). A temperature sensor that measures the copper temperature can be used to correct this error. However, one has to be aware that the thermal resistance between the copper trace and the temperature sensor may lead to an underestimation of the copper temperature [13], [14]. This underestimation can cause a considerable measurement error as demonstrated in Fig. 5. A technique to compensate for the thermal resistance has been proposed that notably reduces the measurement error [14]. Another technique that works without temperature sensing has been proposed especially for power converter applications, in which the input current of the

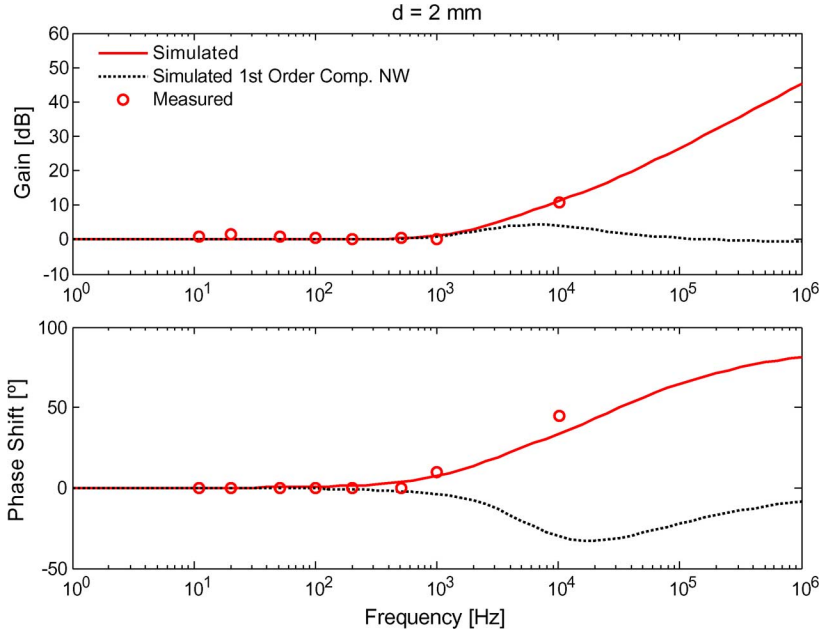

Fig. 6. Bode plot of the measurement bandwidth of the copper trace current sense method with and without compensation network at a distance of 2 mm between forward and return current paths.

converter is used to track the thermal drift of the copper trace [15]. This technique is limited to power converter applications, and does not work properly below 20% of the rated nominal current range.

It should be noted that it is impossible to control the resistance of a copper trace or busbar with satisfactory precision during production process. So, in order to get a sensor signal with 1% absolute error at 25 °C, it is necessary to calibrate the sensor signal, and then combine the measurement of the voltage drop with the correction for the temperature of the busbar. The mutual inductance between sense and main loop together with the skin effect will limit the bandwidth of this current sensing approach [14]. The frequency response of an exemplary busbar arrangement based on simulation and measurements is depicted in Fig. 6. The return conductor was located parallel to the forward conductor with a separation distance of 2 mm. The mutual inductance dominates the frequency behavior, which makes it possible to improve the performance by employing a first-order low-pass filter as a compensation network, similar to the compensation in shunt resistor applications (Fig. 6). The measurement results in time domain are illustrated in Fig. 7.

Since only a very limited number of publications are available on this method we believe that this technique is only used in niche applications. However, due to the high-cost pressure in the power conversion industry, this method may become more popular as a replacement for shunt resistors in order to reduce power losses and to increase power density.

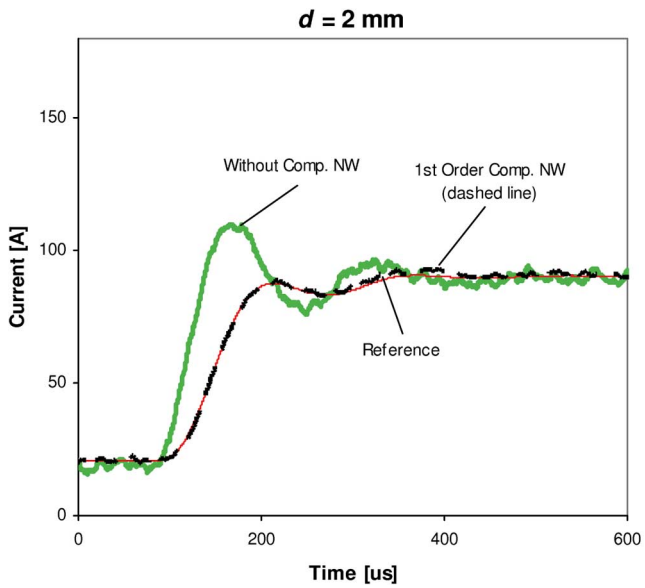

Fig. 7. Measurement of a transient current pulse using the copper trace sense method. The voltage drop across the copper trace exhibits a considerable overshoot due to the mutual inductance between the sense and main loop that can be corrected using a simple first-order low-pass compensation network.

C. Conclusion for Current Sensor Based on Ohm's Law of Resistance

Ohm's law of resistance provides the simplest way to measure currents. A significant drawback of this kind of current sensor is the unavoidable electrical connection between the current to be measured and the sense circuit. By employing a so-called isolation amplifier, electrical isolation can be added. However, isolation amplifiers are expensive. As an example, an integrated circuit (AD202) comes at an approximate price of around 30 USD at 1 k volume. They also deteriorate the bandwidth, accuracy, and thermal drift of the original current sensing method. For these reasons, current sensing techniques based on physical principles that provide inherent electrical isolation normally provide better performance at lower cost in applications where isolation is required.

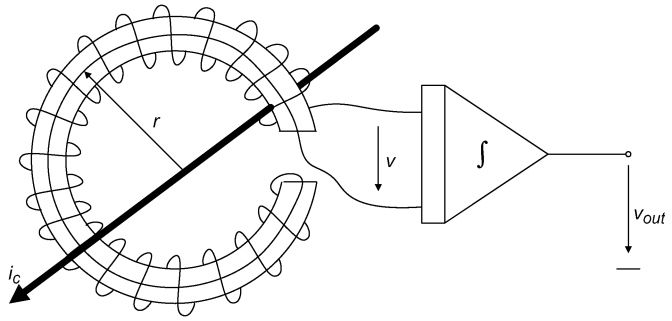

Fig. 8. Schematic of a Rogowski coil that uses a nonmagnetic core material. An integrator is required to get a signal proportional to the primary current i_c from the induced voltage.

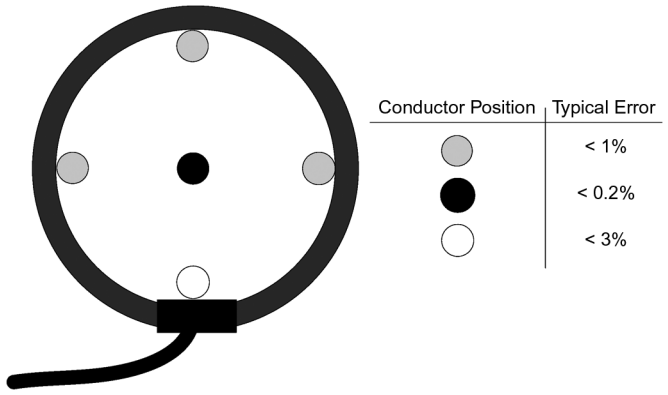

Fig. 9. The influenced of the conductor position on the accuracy of the Rogowski coil.

III. Current Sensors That Exploit Faraday's Law of Induction

Current sensors based on Faraday's law of induction are one example of sensors that provide inherent electrical isolation between the current we want to measure and the output signal. Electrical isolation enables the measurement of currents on a high and floating voltage potential by providing a ground-related output signal. In many applications safety standards demand electrical isolation, and thus make isolated current sensing techniques mandatory.

A. Rogowski Coil

The Rogowski coil displayed in Fig. 8 is a classical example of an application based on Faraday's law of induction. The working principle can be explained starting with amperes law that defines the path integral of the magnetic flux density B inside the coil

$$\oint_C \vec{B} \cdot d\vec{l} = \mu_0 i_C. \tag{4}$$

The current i_C flows through the area enclosed by curve C. To allow a simple theoretical analysis, we assume that the cross section diameter of the Rogowski coil is much smaller than its radius r. This assumption is valid for most coil designs. If the current i_C is centered inside the coil, the magnetic flux density B can be simplified to

$$B = \frac{\mu_o i_C}{2\pi r}. \tag{5}$$

We can apply Faraday's law of induction to determine the induced voltage into the Rogowski coil due to a change in the current i_C

$$v = -N\frac{d\phi}{dt} = -NA\frac{dB}{dt} = -\frac{NA\mu_0}{2\pi r}\frac{di_C}{dt}. \tag{6}$$

A is the cross sectional area of the coil body which is formed by the windings, and N the number of turns. Voltage v is proportional to the derivative of the primary current i_C that we want to measure. An integrator with integrating constant k, and infinitely high input impedance can yield the exact result

$$v_{\text{out}} = -\frac{NA\mu_0}{2\pi r} k \int_t \frac{di_C}{dt} \cdot dt + v(0)_{\text{out}} = -k\frac{NA\mu_0}{2\pi r} i_C + v_{\text{out}}(0). \tag{7}$$

Equation (7) is also theoretically valid if the coil is not centered around the conductor or the coil shape is not circular [16]. By having a look into the datasheet of a commercial Rogowski coil, however, we find that the typical measurement error is increased if the coil is not centered, as shown in Fig. 9 [17]. This is due to the fact that in reality the winding density around the coil is never perfectly constant. Accordingly, the poorest accuracy is obtained if the conductor position is close to the clip together mechanism, where the winding density cannot be even.

Although (7) implies that the Rogowski coil can also measure direct currents, we have to keep in mind that the basic principle is based on the detection of a flux change, which is proportional to a current change. Without knowing what the current was at $t = 0$, which is represented by $v_{\text{out}}(0)$ in (7), it is impossible to reconstruct the DC component. Since practical integrators are not perfect and may exhibit a small but steady input offset voltage, its frequency response has to be altered, so that the gain at low frequency is reduced. Hence, practical Rogowski coils are not suitable to measure low-frequency currents (Fig. 10) [16], [18], [19]. For this reason, it has been recently proposed to combine the Rogowski coil with an open-loop magnetic field sensor that provides the DC information to extend the measurement range to direct currents [20].

While active integrators allow almost freely adjustable integrator gains, they limit the maximum rise time and exhibit saturation at high output voltages. The rise time performance can be improved by using passive integration at the cost of lower gain k. For highest performance, a Rogowski coil with current output has been proposed that exploits its self-inductance for passive integration [18]. Other research has focused on integrating the Rogowski coil into a PCB in order to reduce its bulk [21].

The sensitivity of the Rogowski coil is small compared to a current transformer, because the current transformer can take advantage of the high permeability of the magnetic core material. This can be compensated for by adding more windings

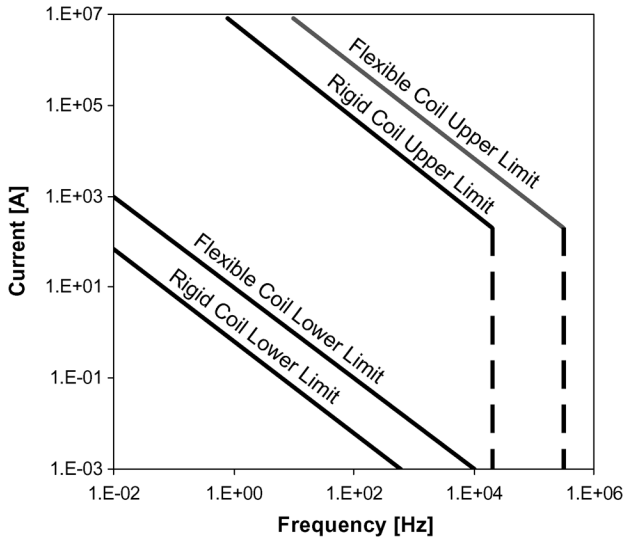

Fig. 10. Current/Frequency limits of Rogowski coils. Rigid coils have the advantage of being able to measure at smaller frequencies, whereas flexible coils have improved handling capability, and usually can measure at higher frequencies.

on the Rogowski coil or using a higher integrator gain k. However, more windings increase the self-capacitance and self-inductance, whereas a higher integrator gain requires an amplifier with large gain-bandwidth product.

The Rogowski coils thermal drift is determined by the integrator but also by the fact that due to the thermal expansion of the coil the cross-sectional area A of the coil body may change. Vibrations can lead to a similar effect because of sliding turns on the coil. Dupraz *et al.* mitigated these problems by integrating the coil windings into a PCB [22].

Rigid coils usually have a higher sensitivity since they allow more turns than flexible coils, and thus provide a lower cutoff frequency, as illustrated in Fig. 10. On the downside, they do not provide the exceptional handling capability of flexible coils, and the large number of turns deteriorates the high-frequency performance.

A distinct feature of the Rogowski coil is that it does not exhibit saturation, and is inherently linear [16], [18]. This makes it especially useful in situations were the amplitude of the current pulse is unknown. Rogowski coils can be applied to measure currents in power distribution systems, short-circuit testing systems, electromagnetic launchers, slip-ring induction motors, and lightning test facilities. The cost is comparable with that of current transformers but with the advantage of less insertion impedance and, in the case of flexible coils, higher user-friendliness.

B. Current Transformer (CT)

Similar to the Rogowski coil, the current transformer (CT) also exploits Faraday's law of induction to measure currents. The construction is basically the same as the Rogowski coil, with one single primary turn and multiple secondary turns but employs a core material with high relative permeability (Fig. 11). The main difference between a CT and a Rogowski coil is that the secondary winding of the current transformer

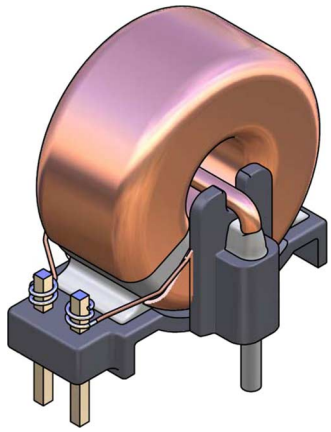

Fig. 11. A current transformer consisting of one primary turn and multiple secondary turns so as to reduce the current flowing on the secondary side (image courtesy Power-One, Inc.).

is loaded with a sense resistor R_s. The current i_s through R_s generates a magnetic flux that acts to counter the flux generated by the primary current. We can modify (6) derived for the Rogowski coil as follows:

$$v_s = -N\frac{d\phi}{dt} = -NA\frac{\mu_0\mu_r}{l_m}\left(i_c - Ni_s\right)\frac{d}{dt} \tag{8}$$

where A is the cross-sectional area of the core. This equation can be solved for i_s

$$i_s = \frac{i_c}{N} - \frac{l_m}{N^2 A\mu_0\mu_r}\int_t v_s \cdot dt. \tag{9}$$

The second term of (9) can be interpreted as an inductance and is commonly known as the magnetizing inductance L_m

$$i_s = \frac{i_c}{N} - \frac{1}{L_m}\int_t v_s \cdot dt. \tag{10}$$

Based on (10), we can construct the equivalent circuit diagram of a current transformer using a theoretical DC transformer [Fig. 12(a)]. It has to be noted, that this equivalent circuit is very basic and neglects stray inductances, core losses, and winding resistance. However, it can be easily justified with the above equations, and gives sufficient insight to understand the current transformer working principle. The capacitor C_w has been added to model the secondary winding capacitance. The importance of this capacitance will be described below.

The second term in (10) also models the inability of the CT to measure direct currents. If the primary current i_c contains a DC component then the magnetizing current i_m will increase until the full DC component flows through L_m [Fig. 12(a)]. So, in the standard configuration, the current transformer is incapable of measuring DC currents. On the other hand, if the second term in (10) is small, which is true when the frequency is relatively high, then the secondary current is directly proportional to the primary current i_c, and can be measured by means of a shunt resistor R_s, as depicted in Fig. 12(a). This gives a current sensor that provides isolation, low losses, simple working principle, and a voltage output that does not need further amplification.

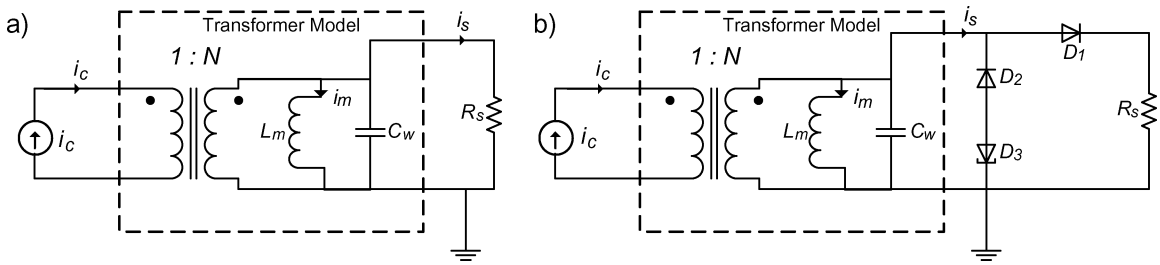

Fig. 12. Equivalent circuit diagrams for current transformers (a) includes a magnetizing inductance L_m, which requires the mean voltage applied to the transformer winding to be zero, or the transformer saturates. The secondary winding capacitance C_w limits the bandwidth, especially at high number of secondary turns. (b) CT where diodes $D_1 - D_3$ allow the transformer to demagnetize during the off-time and protect the sense circuitry that acquires the voltage across R_s.

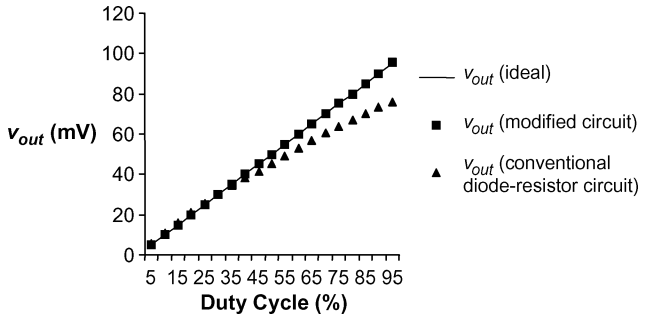

Fig. 13. Output voltage versus duty cycle for a CT. Due to the droop effect, the linearity of the current transformer is degraded at high duty cycle or current pulse with large on-times ($v_{\rm out}$ is the low-pass filtered sense voltage v_s). The method proposed by McNeill *et al.* reduces the excursion of the flux within the magnetizing inductance, and thus leads to a superior linearity [23].

Having an output voltage directly proportional to the primary current is one advantage of a current transformer over the Rogowski coil since no integrator is required that may deteriorate the accuracy by its offset drift or output saturation. The influence of the position of the current carrying conductor is also significantly reduced. The output voltage can be directly sampled by an analog-to-digital-converter. The losses within R_s can be kept low by employing a high number of secondary turns N.

The magnetizing current through L_m can cause a measurement error because this current bypasses the sense resistor, and does not contribute to the voltage drop across R_s. This phenomenon is called droop and refers to the decreasing sense voltage when a current pulse with large on-time is applied at the primary side. According to (9), the droop effect can be mitigated by using a core with high relative permeability or using a smaller sense resistor value since $v_s = i_s R_s$ [7]. The other parameters are seldom changed since they either hurt the physical dimensions (A), the secondary winding capacitance $C_w(N)$ or are difficult to modify (l_m). The core permeability can be increased and is solely dependent on the material available, and the price that is paid for it.

McNeill *et al.* in [23] and [24] proposed the use of an active load on the secondary side that reduces the apparent sense resistance R_s to almost zero. The droop is then mainly determined by the resistance of the secondary transformer winding, and thus is strongly reduced. Fig. 13 shows the difference between the proposed active load and conventional resistive load within a power converter application. The primary current was switched with increasing duty cycle in order to increase the on-time of the current pulse. The conventional circuit shows significant deviation from linear behavior at high duty cycles due to droop.

The engineer has to be aware that the magnetizing inductance L_m is not ideal, and exhibits hysteresis and saturation, which is determined by the core material. For this reason, one has to make sure that the peak magnetizing current does not saturate the transformer core material, and that core losses do not cause the transformer to overheat. The thermal resistance between the transformer core and air is high, so that even small power dissipation in the CT can lead to overheating.

If the primary current is chopped, which is the case in switched mode power converters, the time where the primary winding is disconnected from the circuit can be used to let L_m demagnetize itself through diodes D_2 and D_3 with a circuit shown in Fig. 12(b). This avoids saturation of the magnetizing inductance L_m and allows it to measure direct currents [9]. Using this principle it is possible to measure the output current of a power converter by sensing the current through the MOSFET's with a current transformer [25]. Diode D_1 in Fig. 12(b) protects the measurement circuitry connected to the sense resistor from the negative voltage, which appears at the secondary winding during the demagnetization process. Since the mean voltage across the magnetizing inductance has to be zero, sufficient time needs to be available to reset the core magnetization. This has implications on the maximum allowed duty cycle of the switched mode power converter. Principally, the zener voltage of diode D_3 can be adjusted in order to reduce the demagnetization time. In practice, however, the secondary winding capacitance C_w limits the rise time of the voltage across the secondary transformer winding. The technique of McNeill *et al.* mentioned above is useful here as well since it substantially reduces the reverse voltage that has to be applied to demagnetize the transformer core. This improvement comes at higher cost, and the bandwidth of the current sensor becomes dependent on the performance of the active load.

Despite the described shortcomings, current transformers are very popular in power conversion applications because of their low cost, and the ability to provide an output signal that is directly compatible with an analog-to-digital converter. They are also intensively employed in power distribution networks at 50/60 Hz line frequency.

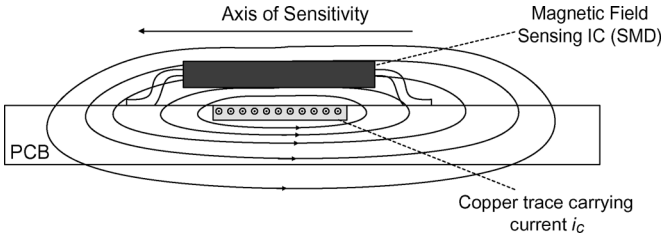

Fig. 14. The simplest schematic for open-loop current measurement. It uses a magnetic field sensor that directly measures the magnetic field around the current carrying conductor. External magnetic fields significantly deteriorate the accuracy of this technique.

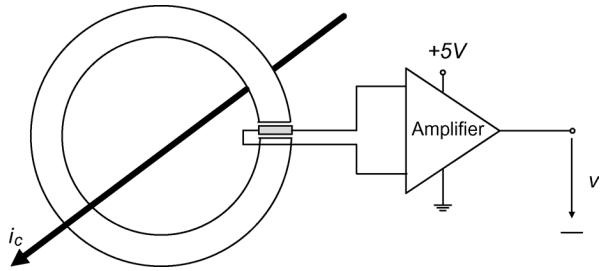

Fig. 15. Schematic for an open-loop current sensing configuration using a magnetic core to concentrates the field from the primary conductor onto the magnetic sensor. This not only increases the sensitivity of the current sensor due to the permeability of the core material but decreases the sensitivity to external magnetic fields.

IV. Current Sensing by Means of Magnetic Field Sensors

In the previous section, we discussed current sensors that exploit Faraday's law of induction. Due to the nature of this law it is impossible to sense currents that generate static magnetic fields. Magnetic field sensors, on the other hand, are able to sense static and dynamic magnetic fields. For this reason, they provide an attractive alternative basis for sensing currents. This section first explains the different sensing configurations. Three different configurations are normally used to build a current sensor based upon magnetic field sensing devices. These are open-loop, closed-loop and a third method that combines magnetic field sensor either with a current transformer or Rogowski coil. After the explanation of the available sensing configuration, the most popular magnetic field sensing technologies are explained.

A. Sensing Configurations

1) Open-Loop Technology: The open-loop configuration provides a simple method to use a magnetic field sensor for current sensing. Fig. 14 shows the basic principle, where a magnetic field sensor that may be integrated into a SMD IC (integrated-circuit) is placed in close vicinity to the current carrying conductor. This principle has the advantage of being simple, inexpensive and compact. It assumes that the magnetic field around the conductor at a certain distance is proportional to the current at all times. The sensitivity, linearity and thermal drift are generally determined by the magnetic field sensing principle.

There are several disadvantages to the open-loop technique. First, in order to achieve high precision *in situ* calibration is required to determine the factor of proportionality between magnetic field and current. The measurement bandwidth is not necessarily limited by the sensing technology but by the required level of amplification of the output voltage. If the sensor is located close to the current carrying conductor, the measurement accuracy may be further reduced by the skin effect, which forces high-frequency current to flow along the outer edges of the conductor, and thus changes the magnetic field at the sensor. The most serious limitation, however, is the susceptibility to stray external magnetic fields. These fields can significantly disturb the measurement accuracy. As an example, permanent magnets and inductors can easily disturb the output signal by several percent even if they are separated by more than 10 centimeters from the field sensor. It is possible to shield against these fields but shielding is complicated, needing to shield against both static and dynamic fields. These shields employ materials with high conductivity and high permeability. Moreover, the presence of a magnetic shield will also change the magnetic field at the sensor's position, exhibit losses due to eddy currents, and change its permeability based on the offset magnetization and frequency. All this makes it very complicated to obtain a linear and reproducible relation between the current and measured magnetic field over a wide frequency range.

A slightly more complex sensor is based upon a magnetic core that is placed around the conductor to concentrate the magnetic field from the primary current i_c onto the magnetic field sensing device (Fig. 15). This significantly reduces the influence of external magnetic fields, increases the sensitivity thanks to the high relative permeability of the core and eliminates the need for *in situ* calibration in order to determine the constant of proportionality between the current and magnetic field. Moreover, the skin effect within the conductor has no influence on the current sensing accuracy.

The performance of this kind of current sensor is not only determined by the type of magnetic field detection but also by the properties of the magnetic core material. Core losses usually limit the measurement bandwidth of this sensing principle below the capabilities of the magnetic field sensing device. The losses are a combination of hysteresis and eddy current losses, and can lead to excessive heating. Many commercial available transducer based on this principle require a down rating of high frequency currents in order to avoid overheating. In addition, an excessive overcurrent situation can saturate the magnetic core material causing a change in the operating point of this sensor. This effect is known as magnetic offset, and causes a constant offset voltage on the output signal. This offset voltage can lead to an absolute error higher than 1% and is permanent. It is possible to retrieve the initial operating point by degaussing the core. This involves driving the core from negative to positive magnetization in decreasing amplitude, illustrated in Fig. 16 [26]. The fringing field around the core gap may also induce a parasitic voltage into the measurement electronics.

2) Closed-Loop Technology: In a closed-loop configuration, the output voltage of the magnetic field sensor is used as an error signal to compensate the magnetization inside the magnetic core by forcing a current i_s through a second transformer winding. This current generates a magnetic field that opposes

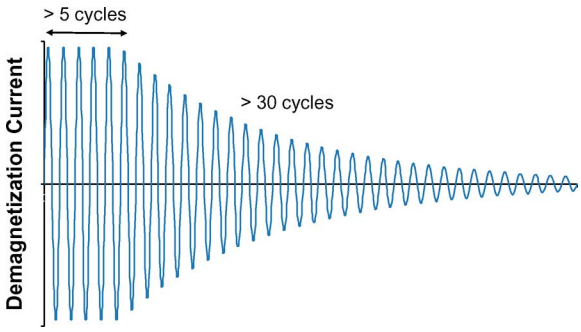

Fig. 16. A degaussing cycle, which consist out of a sinusoidal decreasing demagnetization current, is used to retrieve the initial operation point of the magnetic core material after an overcurrent incident.

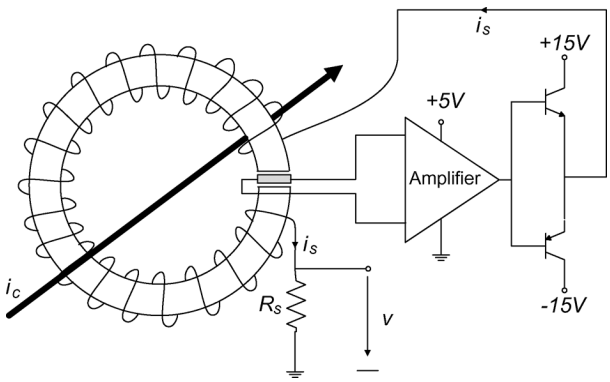

Fig. 17. A closed-loop configuration in which a secondary winding is used to compensate the flux inside the transformer to zero, while the output voltage of the magnetic field sensor acts as an error signal. The current through the secondary winding can be measured to determine the magnitude of i_c.

the primary current i_c, as illustrated in Fig. 17. Assuming the current i_s perfectly compensates the magnetic flux, i_s is proportional to the primary current i_c. This technique greatly reduces the influence of the thermal drift of the magnetic field sensing device. The linearity also becomes independent of the magnetic field sensor. There will still be some offset voltage present due to the amplification stage and the remanence of the core material that may cause some temperature dependent drift. Excessive overcurrent can also change the offset voltage of this measurement principle, and has to be removed by a degaussing cycle. At high frequencies, the secondary winding can act as a current transformer to increase the measurement bandwidth. Fig. 18 demonstrates how the measurement electronic can combine the output signals of the two operation principles to provide an output signal with high bandwidth [26]. At the intersection of these two working principles the frequency response is deteriorated by around 1 dB.

Another benefit of the closed loop sensor is that because the core magnetization is theoretically zero there are no eddy current or hysteresis losses. In reality, a small core magnetization will occur leading to some core losses but they will be significantly reduced compared with open-loop technology. The disadvantages of closed-loop technology are more complicated construction, larger cost, and increased bulk. Another significant disadvantage is that a higher supply current with a supply

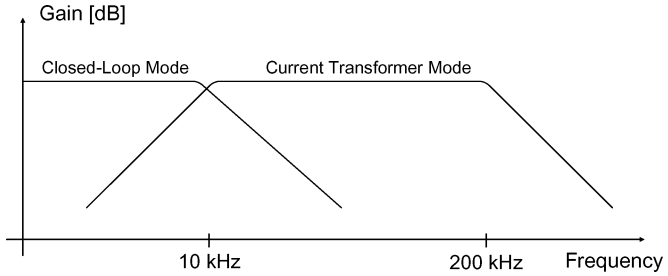

Fig. 18. Use of the secondary winding of a closed-loop configuration as a current transformer to achieve high bandwidth.

voltage of ± 15 V is generally required, so that the magnetic flux can be fully compensated [26].

For some magnetic field sensing technologies, e.g., the anisotropic magneto resistance (AMR), the closed-loop principle discussed above is not suitable, since it requires the field sensor to be very flat in order to reduce the magnetic fringing field around the core gap and to obtain a high apparent permeability. However, a closed-loop current sensing method has been developed, which works without a magnetic core, as shown in Fig. 19. Four magnetic field sensing devices, in this case AMR based, are arranged in a Wheatstone bridge to compensate for thermal drift. The field generated by the primary current i_c is compensated with the magnetic field of a compensation current I_{comp}. The Wheatstone bridge provides an error signal that the control loop tries to reduce to zero. The current I_{comp} is finally measured to determine the magnitude of the primary current. This principle achieves similar performance as compared to the conventional closed-loop principle using a magnetic core, and offers the advantages of smaller size, no magnetic offset and no core losses. However, the immunity against external magnetic stray fields is not as good as the closed-loop principles using a magnetic core material, and the skin effect inside the conductor may alter the magnetic field, which deteriorates the bandwidth of this current measurement principle. For the best precision, the copper trace carrying the current to be measured should be part of the current sensor module, and thus the losses of this copper trace also have to be taken into account. At currents beyond 100 A, these losses can significantly exceed the losses caused by the magnetic field sensing device.

3) Combination of Multiple Techniques: Compared with current transformer and Rogowski coil, current sensing techniques based on magnetic field sensors have the advantage of being able to measure DC currents. Apart from the fluxgate principle mentioned below, however, they do not approach the accuracy and bandwidth of the CT and Rogowski coil. For this reason, it makes sense to merge the advantages of both techniques by combining them.

An example of this is the "Eta" current sensing principle developed by the company LEM. They combined an open-loop magnetic field sensor, in this case a Hall-effect device, using a magnetic core with the CT principle, as shown in Fig. 20. Since no compensation current is required, the power consumption has been greatly reduced, and the sensor can work with a unipolar power supply [26]. At the same time, it is claimed that the Eta technology achieves almost the same performance as

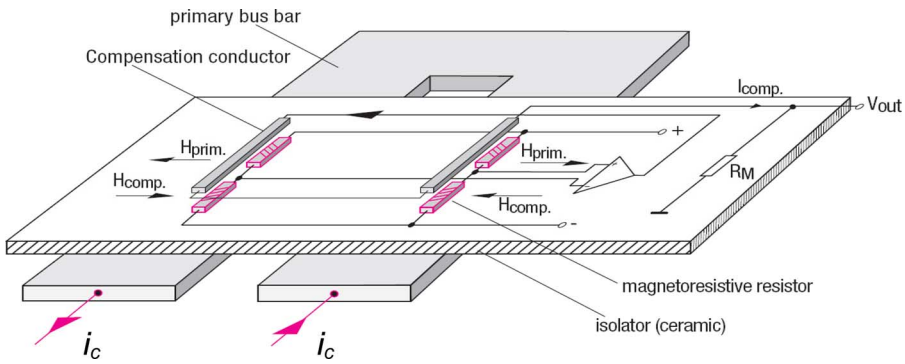

Fig. 19. A closed-loop configuration not using a magnetic core employs a Wheatstone bridge built with magnetic field sensors that measures the superposition of the magnetic fields between the primary current, and the compensation current I_{comp}. The compensation current is adjusted until its magnetic field compensates the field of the primary current. When the magnetic fields compensate each other, the compensation current provides a measure for the primary current (Image courtesy Sensitec GmbH).

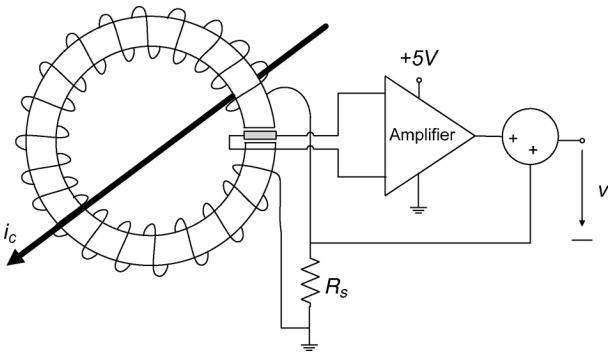

Fig. 20. A schematic of the Eta technology, which combines the output of an open-loop Hall-effect sensor and a current transformer to achieve a high bandwidth current transducer. This greatly reduces the power consumption and enables the use of a 5 V supply voltage compared with ± 15 V for closed-loop sensors.

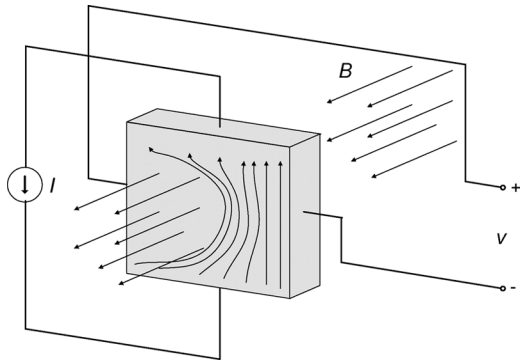

Fig. 21. Due to the Lorentz law, a flowing current I through a thin sheet of conductive material experiences a force if an external magnetic field B is applied. Therefore, at one edge of the sheet the density of conductive carrier is higher, resulting in a voltage potential v that is proportional to the magnetic field B.

the closed-loop principle. The current transformer covers the high-frequency range and the open-loop Hall-effect element provides the low-frequency current information. In general the Eta technology-based current transducers are as expensive as closed loop Hall-effect current transducers.

The combination of magnetic field sensor and CT has been pushed further to build so-called active current probes. These current sensors achieve a measurement bandwidth up to 100 MHz and accuracy around 2% [7]. A planar sensor based on a combination between CT and open-loop Hall-effect technology has been described by Dalessandro *et al.* in [27] and Poulichet *et al.* in [28]. Other designs use a Rogowski coil to measure the high-frequency part of the current [20]. Active current probes are complex in design, large in size and fairly expensive. Therefore, they are typically used in measurement equipment, and are not suitable for mass production. It should be noted that these combination techniques, if they use a magnetic core, will need to degauss the core if a high overcurrent situation occurs.

B. Magnetic Field Sensors

1) Hall-Effect Sensor: One of the most popular magnetic field sensors is the Hall Effect sensor. This sensor is based on the Hall-effect, which was discovered by Edwin Hall in 1879. He found that when a current I flows through a thin sheet of conductive material that is penetrated by a magnetic flux density B, a voltage v is generated perpendicular to both the current and field (Fig. 21)

$$v = \frac{IB}{nqd} \tag{11}$$

where q is the charge of the current carrier, n the carrier density and d the thickness of the sheet. It is interesting to note that the Hall-effect can be explained with the second term in (1) that is neglected in Ohm's law of resistance. This equation is valid for materials in which the electrical conductivity is mediated by either positive or negative charge carriers. This is the case for conductors, while for semiconductors a more complex coherence exists. For this reason, the material properties are collected in the Hall coefficient R_H [29]

$$R_H = \frac{1}{nq}. \tag{12}$$

Indium antimonide (InSb), indium arsenide (InAs), and gallium arsenide (GaAs) are examples of materials that are used in commercial Hall sensors [30]. Their typical performance is depicted in Table I [31]. The ohmic resistance is also an important property, defining the power loss occurring inside the sensor due to the constant current I. Hence, there is a tradeoff between Hall

TABLE I
TYPICAL SENSITIVITY AND THERMAL DRIFT OF COMMERCIALLY AVAILABLE HALL SENSORS

Compound	Sensitivity [V/A·T]	Thermal drift [ppm/K]
Bulk InAs	1	≈ 3,000
Thin Film InAs	10	≈ 3,000
GaAs	20	≈ 3,000
InSb	1,600	≈ -20,000

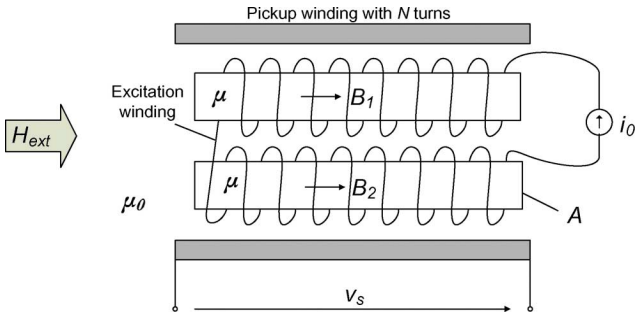

Fig. 22. The Vacquier fluxgate principle: A sinusoidal current i_0 periodically drives the core magnetization from positive to negative values, and thus changes the differential permeability seen by the external field $H_{\rm ext}$. The voltage v_s induced into the pickup winding is measured to determine the magnetic field $H_{\rm ext}$.

plate thickness d, which determines the sensitivity, and the Hall plate resistance.

Another problem related to the Hall-effect sensor can be seen within Fig. 21: The magnetic flux density B also penetrates the area enclosed by the sense wires. Accordingly, a voltage is induced that makes it difficult to sense fast changing magnetic fields. This can be solved by either routing the sense wire behind the Hall plate in order to minimize the active area or by artificially creating an additional loop with the same area but opposite polarity, so that the induced voltage cancels out [31].

At zero magnetic field, an offset voltage is present at the output, also known as misalignment voltage. To use the Hall-effect as a current sensor, additional circuitry is required, particularly to compensate for the misalignment voltage and the distinct thermal drift [32]. Hall-effect sensors are found in open-loop, closed-loop, and combined principles like Eta [26] and active current probes [28]. Advances in semiconductor technologies have led to a steady performance improvement in Hall sensors over the last 50 years. Thus, they are widely used and accepted in current sensing applications. The accuracy is fair for open-loop sensors and high when using the closed-loop configuration. Exemplary applications for Hall-effect sensors are power conversion systems, welding equipment, motor drives, radar devices and in the electrowinning industry.

2) Fluxgate Principle: Fluxgate technology is one of the most accurate magnetic field sensors available today [33] with patents dating back to 1931 [34]. The basic fluxgate principle exploits the nonlinear relation between the magnetic field, H, and magnetic flux density, B, within a magnetic material. The Vacquier fluxgate sensor is depicted in Fig. 22. The excitation winding gives rise to an excitation field H_0 that drives the magnetization of the two parallel arranged rods periodically between positive and negative values. The crucial point is that the excitation field in the two rods is pointing in opposite directions, so that the pickup winding wound around the two rods does not see the magnetic field generated by the excitation winding. The voltage v_s induced into the pickup winding is then given by the difference between the rate of change of flux in the two rods

$$v_s = -2NA\left(\frac{dB_1}{dt} + \frac{dB_2}{dt}\right) \tag{13}$$

where N is the number of turns on the pickup winding, A the cross-sectional area of one rod. By using a sinusoidal current i_0 to drive the excitation winding, the time dependent rate of change of B in each of the cores can be discussed in terms of their permeability μ given by

$$\mu = \frac{dB_{H_{\rm ext}\pm H_0}}{d(H_{\rm ext}\pm H_0)} \tag{14}$$

where μ is dependent on the field $H = H_{\rm ext} \pm H_0$ because of the nonlinear behavior of the core [Fig. 23(a)]. The shape of the $B-H$ loop given in Fig. 23(a) is the combination of the demagnetizing effects, associated with the geometry of the rods, and the properties of the core material [35]. Combining (13) and (14) yields

$$v_s = -2NA\left(\mu_1\frac{d(H_{\rm ext}+H_0)}{dt} + \mu_2\frac{d(H_{\rm ext}-H_0)}{dt}\right). \tag{15}$$

For static external field $H_{\rm ext}$ (15) becomes

$$v_s = -2NA\frac{dH_0}{dt}(\mu_1 - \mu_2). \tag{16}$$

We can then define the differential permeability μ_d as

$$\mu_d = \mu_1 - \mu_2 = \frac{dB_{H+H_0}}{d(H_{\rm ext}+H_o)} - \frac{dB_{H-H_0}}{d(H_{\rm ext}-H_0)}. \tag{17}$$

The differential permeability μ_d is time dependent due to the time dependent changes in the excitation field H_0 [Fig. 23(b)]. The voltage induced into the pickup windings is then given by

$$v_s = -2NA\mu_d\frac{dH_0}{dt}. \tag{18}$$

Provided that the external field $(H_{\rm ext})$ is small compared to the excitation field (H_0), then the peak in v_s is proportional to external field and can be used to measure the field. Note that in this analysis hysteresis has been neglected but can be modeled as a phase shift between the excitation field, H_0, and the differential permeability, μ_d.

The pickup voltage v_s is generally detected by measuring the second harmonic component. As we can see in Fig. 23(b), the fundamental frequency of the pickup voltage v_s is twice the frequency of the driving field H_0. In closed-loop fluxgates, the pickup voltage serves as an error signal that generates an additional magnetic field that opposes $H_{\rm ext}$ by means of an additional winding or by driving the pickup winding itself.

The sensitivity of the fluxgate method can be improved by using a higher excitation current frequency, more turns on the pickup winding, or a core with a rapidly changing permeability

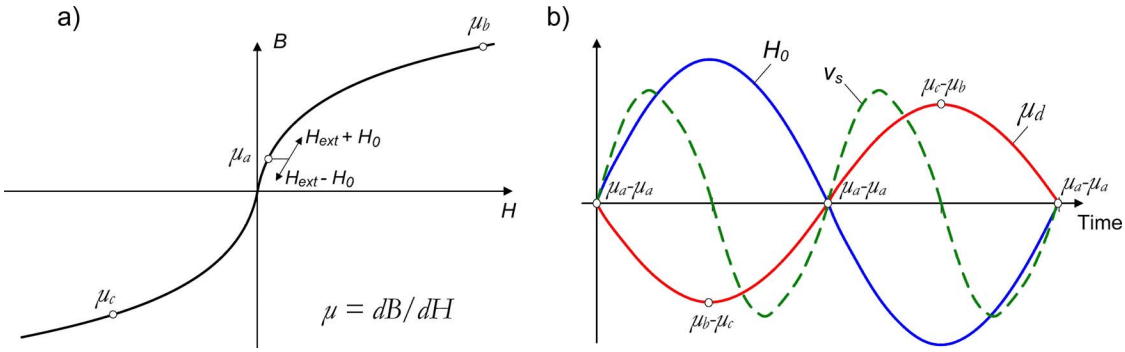

Fig. 23. The fluxgate method takes advantage of the fact that the permeability μ of a magnetic core material depends on the applied magnetic field H.

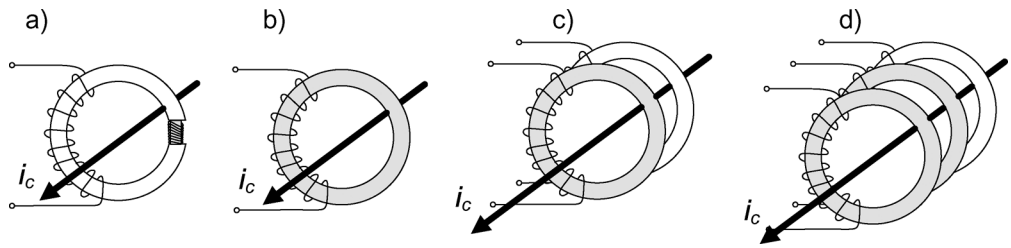

Fig. 24. The fluxgate principle can be used in different ways to measure currents. (a) In a closed or open-loop configuration where the magnetic field sensor is represented by the fluxgate. (b) Low-frequency version using a closed toroid core without pickup winding. (c) Additional current transformer to extend the bandwidth. (d) Having a third core to oppose the voltage disturbance introduced into the primary conductor by the first fluxgate.

μ, i.e., a core with rectangular B-H loop characteristic. However, tradeoffs have to be made since a high excitation current frequency increases eddy currents in the core material, and the distributed winding capacitance increases with N, and may lead to unwanted resonances [36].

Numerous fluxgate principles other than the Vacquier are known, some of them process the output signal in the time domain or have the excitation field orthogonal to the external field H [34]–[37]. The second harmonic detection method, in general, provides the best performance.

A fluxgate allows for some unique techniques to be used to measure currents that cannot be realized using other field sensors. Some popular designs are depicted in Fig. 24. First, the fluxgate-based magnetic sensor can be used in a closed loop or open-loop configuration as discussed above [Fig. 24(a)]. The magnetic field around the primary current i_c is concentrated by the magnetic core. In the closed-loop principle, the secondary winding is used to compensate the concentrated magnetic field. Due to the superior sensitivity and temperature stability of the fluxgate method compared with other magnetic field sensors, high accuracy is achieved.

In another technique a single closed annular magnetic core is used, as shown in Fig. 24(b). In this embodiment, no pickup winding is present, and the current through the excitation winding is examined to determine the magnitude of the primary current i_c [26], [38], [39]. In spite of the low-cost design, the thermal drift of this fluxgate current sensor is still very low as demonstrated in Fig. 25. On the other hand, the bandwidth of this fluxgate configuration is limited by the time required to drive the core between positive and negative saturation.

To increase the bandwidth, the fluxgate can be used together with a current transformer as shown in Fig. 24(c). Here, the fluxgate principle provides the low-frequency current information, while the current transformer is responsible for the high-frequency content. Finally, Fig. 24(d) illustrates the most advanced but also most costly adaptation that uses a third core to compensate for the voltage noise introduced into the primary conductor by the first fluxgate sensor. This voltage noise is in fact nothing else than the voltage applied to the excitation winding multiplied by the turns ratio N, which is visible on the primary side when the magnetic core material is not in saturation, thus acting as a transformer.

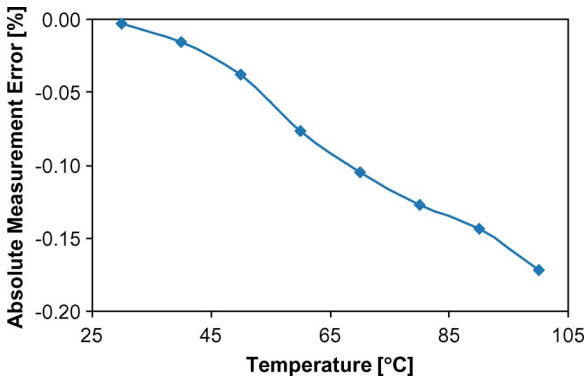

Fig. 25. Thermal drift of a 15 A current sensor based on the fluxgate technology.

Many different current sensors with different names based on the fluxgate principle have been proposed in literature [40]–[43]. These publications mainly deal with different variants of evaluating the pickup winding voltage to determine the current. Recently, an effort has been made to integrate an open-loop fluxgate current sensor with PCB technology

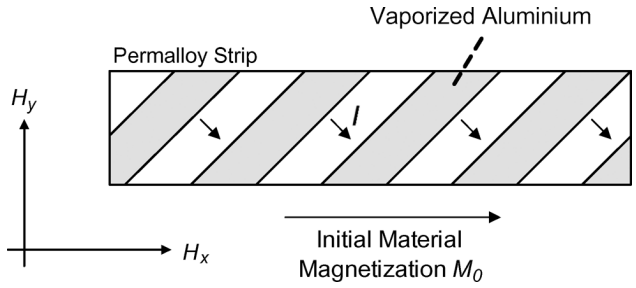

Fig. 26. An AMR Sensor consisting of aluminum is vaporized onto a permalloy strip in a 45° angle against the intrinsic magnetization M_0 so as to cause the current I to flow at 45° to M_0 because of the much lower resistance of aluminum compared with permalloy.

[44], [45]. This is certainly a promising development towards low-cost applications. The achieved linearity for the open-loop sensor was limited to 10% due to the difficulty of integrating windings in PCB technology. Standalone fluxgate sensors are commercially successful but so far only in high precision applications because of the high cost and size requirements. Due to the very high accuracy, fluxgates are often employed in calibration systems, diagnosis systems, laboratory equipment, and medical systems.

3) Magneto Resistance Effect (MR): It is possible to build structures in which the electrical resistance varies as a function of applied magnetic field. These structures can be used as magnetic field sensors. The most common application of these sensors has been as the read head in magnetic recording, but they are now being examined for other potential applications. These resistors are normally configured inside a bridge configuration to compensate for thermal drift. The two most popular MR effects together with the most promising future candidates are discussed below.

a) Anisotropic Magneto Resistance (AMR).
b) Giant Magneto Resistance (GMR).
c) Future candidates.

a) Anisotropic Magneto Resistance (AMR) sensors: The resistance of ferromagnetic materials, such as permalloy (an iron nickel alloy), is related to the magnitude and direction of the applied magnetic field. In particular, a current I that flows through a ferromagnetic material experiences a resistance that is dependent on the angle between the current's flow direction, and direction of magnetization M [46]. The minimum resistance is when the magnetization M is perpendicular to the current I. The resistance reaches its maximum when the current I flows parallel to the magnetization M.

In order to make the AMR effect sensitive to the direction of the magnetic field, the current I is forced to flow at a 45° angle to the field direction via a series of aluminum bars deposited onto a permalloy strip (Fig. 26). This structure, known as barber poles, provides a low impedance path for the current and directs it to flow at 45° to the initial magnetization M_0. The cost of this improvement is a reduction in the sensitivity of the sensor due to a reduction in the change of the resistance.

Fig. 27(a) shows the change in resistance $\Delta R/R$ in relation to the angle θ between the material magnetization M and the current I. The maximum variation of this resistance is very small, normally around 2%–4% [33], [46], [47]. In Fig. 27(b), a ferromagnetic strip is shown together with the direction of current I and the magnetization M. The magnetization M is the superposition between the initial magnetization direction, M_0 and the external applied magnetic field H_{ext}. Due to the barber pole principle, the current I has a 45° offset towards the initial magnetization M_0. If H_{ext} is applied perpendicular to M_0, the resulting magnetization M changes its position. Hence, the angle between the current I and magnetization M changes, and so does the permalloy strip's resistance. Since the current is forced to flow in a 45° angle to the initial magnetization M_0, a bias is generated that allows it to determine if the external field H_{ext} is of positive or negative polarity [Fig. 27(a)]. By using a constant current I, the voltage drop across the permalloy strip is now linear for a certain range of negative and positive values for H_{ext}, which is shown in Fig. 28. Moreover, the sensitivity can be adjusted by generating an artificial magnetic field H_x parallel to the x axis. For higher values of H_x, the angle between the material magnetization M and the current I will change less rapidly with H_{ext}, which is also demonstrated in Fig. 28.

The main problems of AMR sensors are high thermal drift, and high non-linearity. In addition, a strong magnetic field can permanently change the intrinsic magnetization M_0 of the permalloy strip, and thus make the sensor useless until a reorientation of the magnetization has been performed. The basic sensor principle has a thermal drift of 3000 ppm/K, which can be compensated by using the Wheatstone bridge configuration of Fig. 19. Hysteretic and eddy current effects inside the permalloy limit the frequency response of the AMR technique to 1 MHz [46]. In commercial available AMR current sensors, however, the limited gain-bandwidth product of the amplification stage normally limits the frequency response to a few hundred kilohertz (Fig. 29). AMR current sensors are available as open-loop magnetic field sensing devices or closed-loop current sensors in the Wheatstone configuration depicted in Fig. 19. The Wheatstone configuration is currently somewhat more expensive than comparable closed-loop Hall-effect current sensors. AMR current sensors are used in power conversion systems and motor control applications.

b) Giant Magneto Resistance (GMR) sensors: The GMR Effect is another technique used to detect static and dynamic magnetic fields. As with the AMR Effect, the magnetic field has a direct influence on the apparent resistance R of the GMR device. The discoverers Gruenberg and Fert received the 2007 Physics Nobel Prize for this work [48], [49]. The importance of their work is justified by the fact that the GMR Effect exhibits a change in resistance due to magnetic fields up to 12.8% at room temperature compared with 2%–4% for the AMR effect [33]. This means that it is possible to detect magnetic fields up to four times weaker than that measurable with the AMR sensors. This ability has been used to improve the performance of read heads and so increased the data density in hard disk drives. Using the GMR effect, it is now theoretically possible to detect very small currents that were below the detection limit of sensors based on AMR or Hall-effect. At the same time, the GMR technology is supposedly cheaper to produce as the sensors are smaller and can be mass produced using standard semiconductor technology.

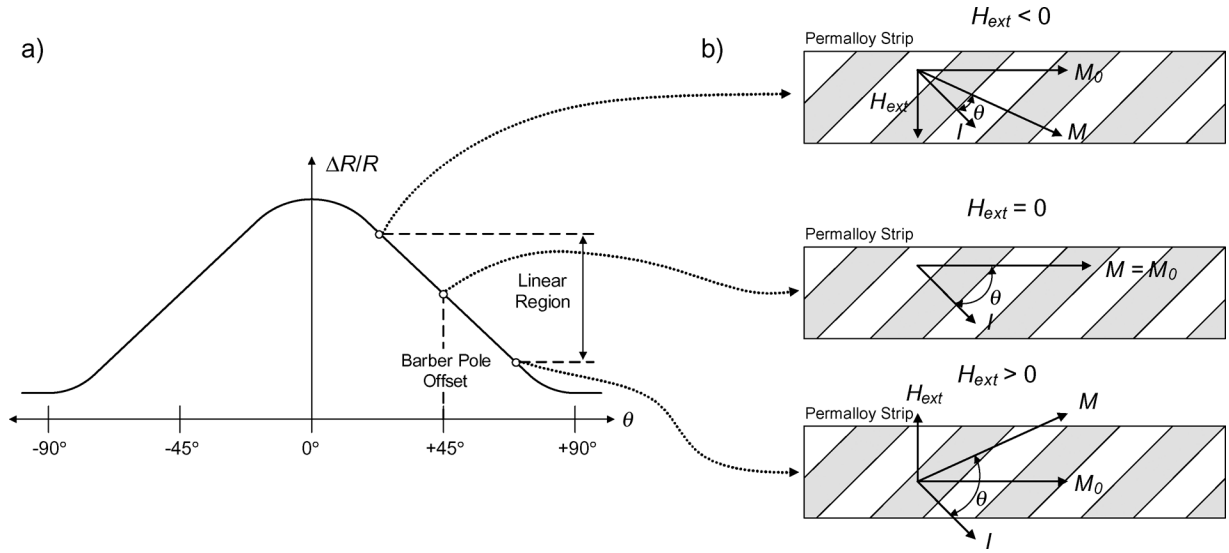

Fig. 27. The change in resistance of an AMR sensor as a function of the angle between the current I and the magnetization M. An external magnetic field $H_{\rm ext}$ causes a change in the direction of M, which is the superposition between M_0 and $H_{\rm ext}$.

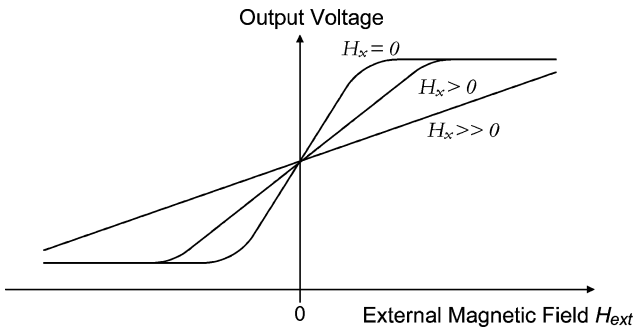

Fig. 28. The output voltage as a function of external magnetic field for an AMR sensor. By applying an auxiliary magnetic field H_x along initial direction of magnetization of the permalloy strip (M_0) it is possible to adjust the field sensitivity of the sensor and suppress saturation effects.

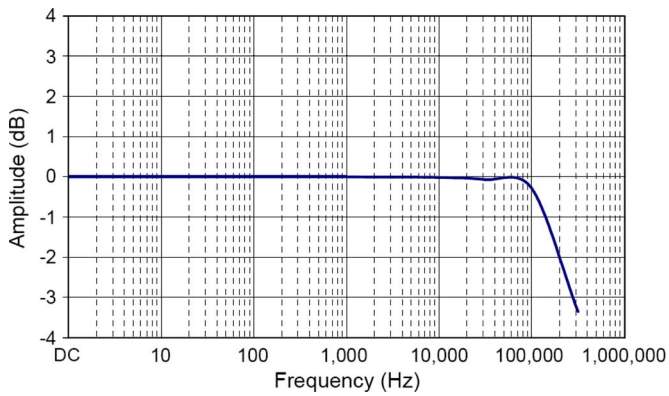

Fig. 29. Frequency response of a commercial available AMR current sensor (Image courtesy Sensitec GmbH).

The basic working principle of the GMR Effect can be explained using the spin-valve structure [50]. It has to be noted that this is just one example of a structure that exhibits the GMR effect [33], [50]. The four-layer structure illustrated in Fig. 30 is just a few tens of nanometers thick and can be integrated into an IC. A thin conductor separates two ferromagnetic layers. One ferromagnetic layer has its magnetization pinned by an antiferromagnetic layer. The magnetization of the free magnetic layer is oriented by an applied external field. If the free ferromagnetic layer is magnetized in the opposite direction to the pinned layer, the resistance R perpendicular to the layers is large [Fig. 30(b)]. The resistance is low when the external magnetic field orientates the magnetization of the free layer so that it is in the same direction as the pinned layer [Fig. 30(c)]. The reason for the change in the apparent resistance R can be explained in terms of spin-dependent electron scattering. In a simplified model we distinguish between spin-up and spin-down electrons. If the free and pinned ferromagnetic layers are pointing into the same direction, only one type of electron is scattered significantly. If the two ferromagnetic layers point in opposite directions, all electrons experience scattering, which results in an increase in the apparent resistance R [51].

Although the GMR technology exhibits many desirable characteristics, there are serious drawbacks that limit its usefulness in current sensing applications. The first problem is the nonlinear behavior and distinct thermal drift. While for digital applications like the read head of a hard drive the nonlinearity is not a problem, a current sensor is supposed to be linear, and thus a correction function needs to be employed. Additionally, a very strong external field can unpin the pinned ferromagnetic layer and permanently alter the sensor behavior [Fig. 30(d)].

At present, commercially available GMR current sensors work according to the core-less open-loop principle (Fig. 14). They are normally configured in a bridge configuration in order to reduce thermal drift. As mentioned before, the skin effect inside the conductor that carries the current to be measured may limit the bandwidth below the bandwidth provided by the GMR sensor itself.

A prototype device has been simulated, designed and produced [52], [53]. The measurement accuracy was found to be limited by the high thermal drift, with a temperature coefficient beyond 1000 ppm/K and by the sensitivity to external magnetic

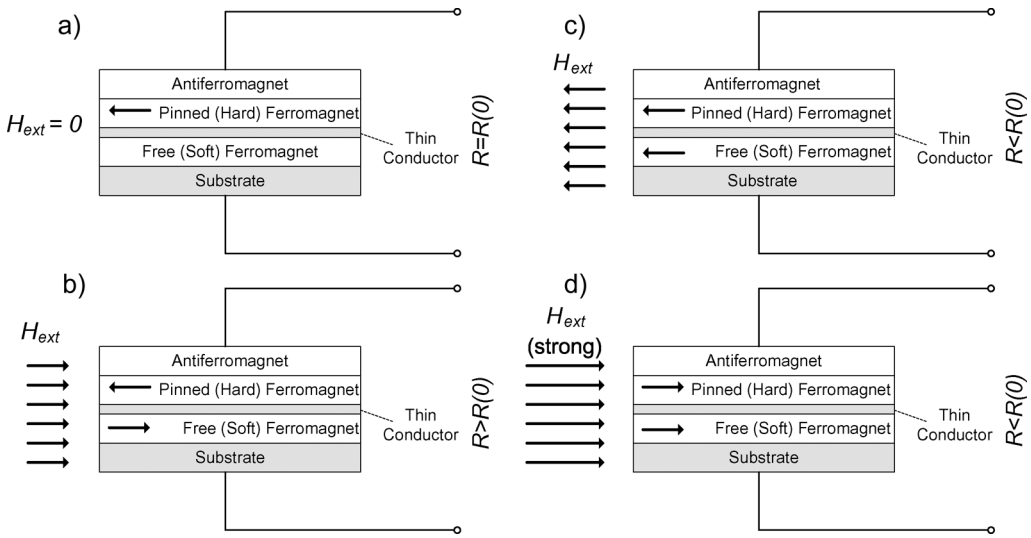

Fig. 30. Basic working principle of the GMR effect: (a) At zero external magnetic field $H_{\rm ext}$, the resistance $R(0)$ appears at the input leads. (b) A magnetic field $H_{\rm ext}$ that points into opposite direction as the intrinsic magnetization of the pinned ferromagnetic layer increases the resistance. (c) The opposite happens if $H_{\rm ext}$ points into the same direction as the pinned ferromagnetic layer's magnetization. (d) The intrinsic magnetization of the pinned ferromagnetic layer can be permanently changed by applying a strong external magnetic field $H_{\rm ext}$.

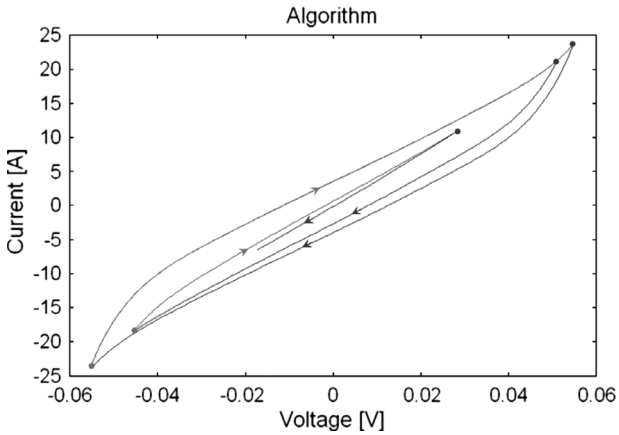

Fig. 31. An example of hysteresis effects within a GMR sensor, which can be compensated by suitable algorithms within the interfacing electronics [55].

fields. Another drawback is that the GMR Effects exhibits notable hysteresis [54]. Fig. 31 shows the measured hysteresis of a GMR current sensor. Attempts have been made to remove the hysteresis by using a sophisticated correction function that has been implemented in a digital-signal-processor (DSP) [55].

Despite these problems, a lot of research is presently being carried out into GMR current sensors. It seems that the potential cost advantage and gain in sensitivity against earlier technologies like AMR and Hall-effect is significant. However, to date commercially available core-less open-loop GMR sensors are still more expensive than comparable Hall-effect and AMR devices. Their fields of application are similar to AMR and Hall-effect based current sensors.

c) Future candidates: In addition to existing field sensors there are a number of other field sensing technologies that may be developed into future current sensors. One interesting candidate is the giant magneto impedance (GMI) effect. It has been observed that the impedance of amorphous ribbon is a strong function of the applied magnetic field and the frequency of the measurement current through the ribbon. At high driving frequencies, the impedance of the amorphous ribbon is solely determined by the external applied field. To use the GMI effect to sense magnetic fields, the ribbon can be included into an oscillator configuration where its impedance influences the oscillator frequency [56]–[58]. The GMI effect is even more sensitive to magnetic fields than the GMR effect.

Tunneling magneto resistance (TMR) based on magnetic tunnel junctions is another potential sensor technology that exhibits substantially higher field sensitivity than existing AMR and GMR sensors. Using the TMR effect, resistance changes up to 230% at room temperature have been reported [59], [60]. The structure and working principle is similar to the GMR principle but uses a 1 nm thick insulator instead of a conductor to separate the two ferromagnetic layers [33].

At this point there are no commercial current sensors based on these techniques available but they have the potential to become more relevant in future due to the very high sensitivity.

C. Conclusion for Magnetic Field Sensors

Current transducers based on Hall-effect field sensors are widely used and accepted due to their capability to measure direct currents whilst providing electrical isolation. The accuracy is fair for open-loop sensors and high when using the closed loop technique. The most serious limitation is the degaussing cycle required after an overcurrent incident, and the distinct temperature related drift of the output voltage. Apart from the AMR sensor, the other field sensing technologies are not employed yet in closed-loop principles. Therefore, they suffer problems typical for open-loop sensors like fairly high thermal drift, poor immunity against external fields, and nonlinearity.

Applications for current sensor based on magnetic field sensing devices are far-reaching and include power conversion systems, welding equipment, motor drives, radar devices and electrowinning industry.

V. Current Sensors That Use the Faraday Effect

Light waves propagating through a medium exhibit a state of polarization that is given by the electric field vector $\mathbf{E}$ as a function of time and location. In the most general case the tip of the $\mathbf{E}$ field vector describes an ellipse. Circular polarization describes the special case where the ellipse becomes a circle, while in linear polarization the ellipse collapses into a line. The state of any polarization can always be described as the superposition of two orthogonal linear or circular polarized light waves. A medium that changes the state of polarization is said to be birefringent. Material having circular birefringence changes the polarization of linear polarized light, and maintains the polarization of circular polarized light. Linear birefringent material behaves *vice versa* [61]. One of Faraday's many discoveries was that circular birefringence can be induced into a material by applying a magnetic field parallel to the light propagation direction. If the intrinsic circular birefringence of a medium is negligible small, the rotation plane of the polarization of linear polarized light is proportional to the integral of applied magnetic field H along the path s

$$\theta = V \int \vec{H} \cdot d\vec{s} \tag{19}$$

where the constant of proportionality V is the Verdet constant, a property of the medium through which the light travels that describes the strength of the Faraday Effect. As mentioned above, linear polarized light can be thought of as being composed of two orthogonal circular polarized light waves. In particular, a linear polarized light wave is the superposition of a right-hand circular polarized (RHCP) light wave orthogonal to a left-hand circular polarized (LHCP) light wave. In the Faraday effect the velocity of the RHCP light waves is decreased if the magnetic field is pointing along its propagation direction, and increased when the magnetic field points in the opposite direction. LHCP light waves behave *vice versa*. This means that if linearly polarized light, which is the superposition of RHCP and LHCP light, is fed into a material undergoing the Faraday effect there will be a phase difference induced between the two different circularly polarized beams, and as a result the polarization plane of the linear polarized light is rotated.

Researchers have been investigating optical current transformers that exploit the Faraday effect for more than three decades [62]. They provide an attractive alternative in applications where excellent electrical isolation is essential, e.g., in power distribution systems. In these applications, the construction of traditional current transformers becomes increasingly difficult and expensive due the requirements placed upon the insulation material that needs to withstand very high voltages, and need to avoid saturating the core material. As an additional benefit, optical current sensors also enable the measurement of direct currents beyond 100 kA. A commercially available 500 kA DC fiber-optic current sensor has been described in [63]. This sensor uses a negligible amount of energy and space compared with existing Hall current sensors that dissipate several kilowatts of power, and can weight more than two tons [64].

A. Polarimeter Detection Method

A straightforward way to use the Faraday effect to measure current is depicted in Fig. 32. Linear polarized light is feed into

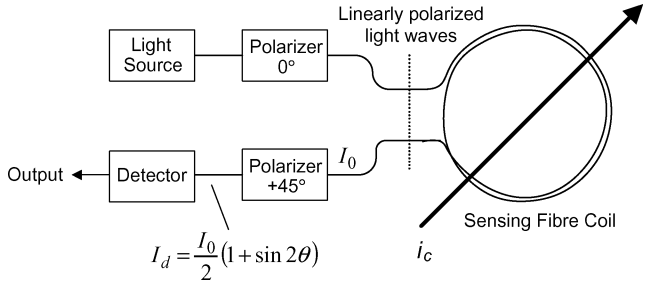

Fig. 32. A schematic of a fiber polarimeter, which is the simplest technique used to measure the current, i_c, using the Faraday technique.

a fiber-optic coil with N turns that encloses the current i_c to be measured. The rotation θ of the linear polarized light can be calculated using Ampere's law

$$\theta = VNi_c. \tag{20}$$

A desirable effect of using a fiber-optic coil is that only magnetic fields due to currents inside the coil are detected as external stray magnetic fields will in general cancel out. Moreover, the position of the current carrying conductor within the fiber-optic coil has no appreciable influence on the measurement accuracy. The analyzing circuit consists of a polarizer at 45° to the original polarization direction so that the output light intensity I_d is given by

$$I_d = \frac{I_0}{2}(1 + \sin 2\theta) \tag{21}$$

where I_0 is the input light intensity. For small rotation θ, the sine function can be linearized. A major problem with the configuration shown in Fig. 32 is the dependence of the output signal on the input light intensity I_0. This problem can be addressed by using a polarizing beam splitter (Wollaston prism) set at 45° so as to split the beam equally, as illustrated in Fig. 33. In this configuration, the ratio between difference and sum of the output I_1 and I_2 of the two detectors is calculated

$$S = \frac{I_1 - I_2}{I_1 + I_2} = \sin 2\theta \approx 2VNi_c. \tag{22}$$

Thus, the output signal S is independent of I_0 [65].

As mentioned before, the linearity of this principle is limited to small rotation θ due to the nonlinear behavior of the sine function at large arguments. The accuracy is further deteriorated by birefringence induced by bending the fiber-optic cable. For this reason, early optical current transformer based on this principle used bulk glass instead of fiber-optic cable to avoid bending stress, which was inflexible, expensive, and limited to a single turn [66]. Today, highly birefringent spun and flint glass fibers are available that are relatively insensitive to stress and make the use of solid glass obsolete.

In contrast to the birefringence induced into the fiber by bending stress, the Faraday effect is nonreciprocal, which means the induced phase shift depends on the direction of the light propagation through the system [67]. This fact can be capitalized upon sending the light along both directions inside the fiber-optic coil and detecting the differential rotation in the polarization (Fig. 34). This method has been discussed by

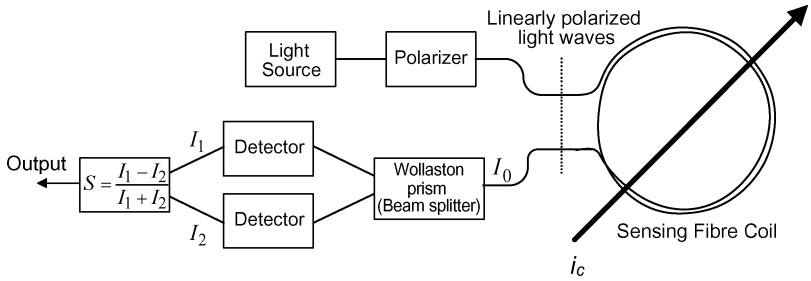

Fig. 33. A fiber polarimeter in which a polarizing beam splitter at 45° to the beam is used to split the beam equally between the two detectors so that the dependence on the light intensity, I_0 can be eliminated.

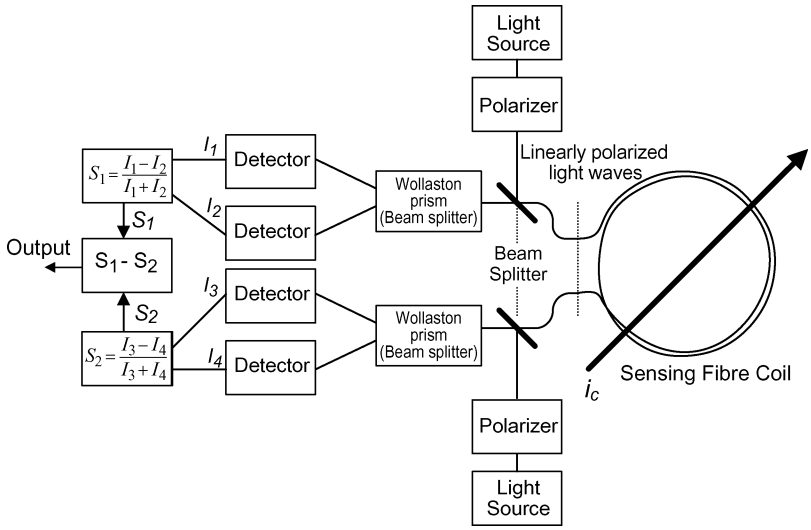

Fig. 34. To eliminate the effect of bending stress on the fiber-optical cables it is possible to send two light beams with different directions through the fiber-optic coil. Bending stress produces a reciprocal phase rotation, which will cancel out on subtraction while the Faraday effect generates a nonreciprocal signal that will not cancel out.

Rogers *et al.* in [68]. However, the measurement range is still limited to $\theta \ll 90°$ due to the nonlinearity of the sine function.

B. Interferometer Detection Method

Another technique used to measure the Faraday Effect is by means of two counter propagating light beams using a Sagnac interferometer. This technique provides a better scale factor stability, excellent zero point stability, and for a closed-loop technique significantly increased measurement range over the polarimeter detection method [63], [69]. The Sagnac interferometer method has been developed for fiber optic gyroscopes that have been continuously improved over many years [62].

Sagnac interferometers accurately measure the phase shift between two linear polarized light waves. The interferometer method can be used for sensing currents by feeding two circular polarized light waves into either end of the fiber-optic cable that encloses the current to be measured (Fig. 35). At exiting the coil, the circular polarized light is converted back into linear polarized light that can be processed by the Sagnac interferometer [67], [70]. As discussed previously, the propagation speed of circular polarized light is altered by the Faraday effect, which means that one light wave travels at increased speed, whereas the other one is slowed down. Therefore, a phase shift between the two light waves results that is a direct measure for the magnitude of the magnetic field or current, respectively.

The Sagnac interferometer linearly polarizes the source light and splits it into two equal beams, which are converted into circularly polarized beams using quarter wave $(\lambda/4)$ retarders. Once the two light beams exit the coil, they are converted back into linear light waves, which now have a phase difference proportional to the current i_c due to the Faraday effect. The differential phase shift $\Delta\phi_s$ between the returning linear polarized light waves can be described according to [70]

$$\Delta\phi_S = VN \oint_C \vec{H} \cdot d\vec{s} = 2VNi_c. \tag{23}$$

As an example, the Faraday effect induces a phase difference of 2.65 $\mu\mathrm{rad/A}$ at a wavelength of 850 nm for fused silica fiber [71]. The open-loop Sagnac interferometer measures the phase shift $\Delta\phi_s$ by bringing the retrieved linear polarized light to interference (Fig. 35) [67]. Using this system the detected interfered light beams may cancel each other at 180° phase shift or lead to a constructive interference at 0°. The detected light intensity I_d resulting from the interference is determined by

$$I_d = \frac{I_0}{2}(1 + \cos\Delta\phi_s) \tag{24}$$

where I_0 is the light intensity of the light source [70]. Naturally, this formula is only an approximation since no losses within the fiber-optic cable and components are considered. A major

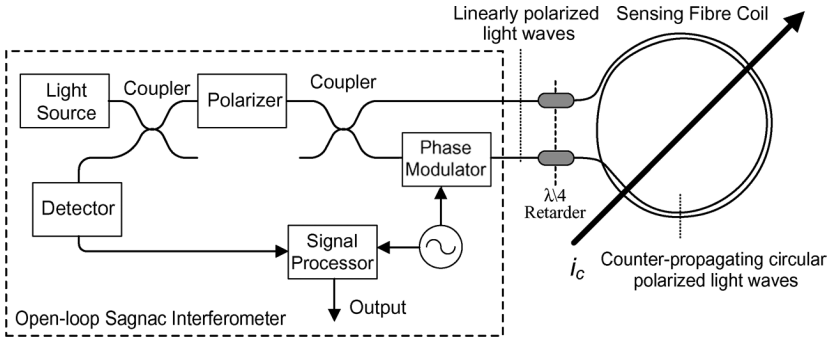

Fig. 35. Schematic of an open-loop Sagnac interferometer that measures the phase shift between circular polarized light waves, which is proportional to the magnetic field. A phase modulator is required to obtain a linear relation between the phase shift and detection signal.

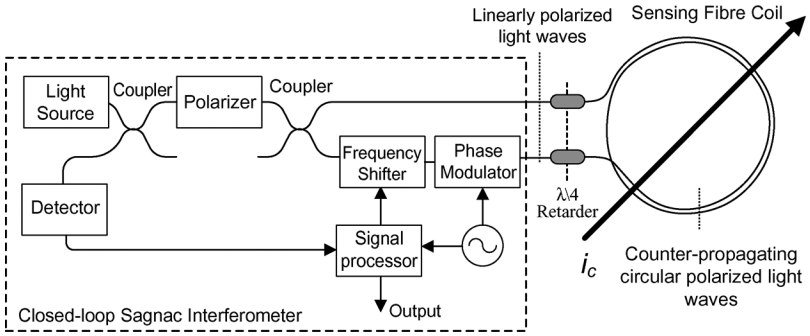

Fig. 36. In a closed-loop Sagnac interferometer the phase shift induced by the Faraday effect is compensated by means of a frequency shifter, and thus achieves a linear response over a much larger measurement range than polarimeter and open-loop interferometer detection methods.

problem of this detection method is the very small sensitivity around $\Delta\phi_s = 0$. For this reason, a periodic phase modulation is carried out, as shown in Fig. 35, that allows it to generate a linear output from the detected signal by building the ratio of the first and second harmonic amplitude level [62], [70]. The phase modulator can be realized by winding fiber around a piezoelectric transducer. However, the measurement is only linear for $\Delta\phi_s \ll 90°$.

The closed-loop method pushes the interferometer approach one step further by compensating the phase shift induced by the Faraday effect by means of a nonreciprocal frequency shifter (Fig. 36). The signal processor implements a control loop that adjusts the phase shift using the frequency shifter until both light beams are in phase. Accordingly, the control signal for the frequency shifter, is a direct measure for the phase shift $\Delta\phi_s$, and is linear over a much larger range than the open-loop principle [62].

Although the method of feeding the light into both ends of the fiber-optic cable enhances the immunity against bending stress inside the fiber, the discussed detection methods are still vulnerable against vibrations and thermal drift of the Verdet constant. In addition, acoustic vibrations at the second and third harmonic are widespread in power distribution systems, and may deteriorate the measurement accuracy of the detection methods [68], [72].

The thermal drift can be compensated by employing a retarder with counteracting temperature behavior or by using a dedicated temperature sensor that allows a compensation within the signal processor [64], [70]. Using these methods, an overall sensing accuracy of better than 0.1% can be achieved, as demonstrated in Fig. 37.

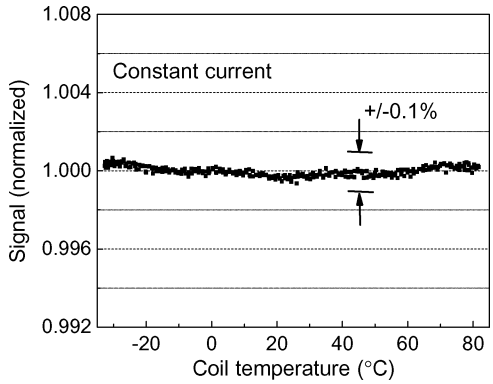

Fig. 37. Temperature dependence of a Sagnac interferometer with temperature compensation, capable of an overall accuracy of better than 0.1% over a wide temperature range [64].

The vibration problem can be eased by using a so-called reflective or in-line sensor arrangement, as shown in Fig. 38 [69], [73]. In this configuration, RHCP and LHCP light waves are fed into the fiber coil from the same end of the coil. At the mirror attached to the other end of the coil, the light beams are reflected and their polarizations states swapped from RHCP polarized to LHCP and *vice versa*. Accordingly, the total phase shift is two times that of the original Sagnac interferometer because the light travels through the coil two times

$$\Delta\phi_S = 4VNi_c. \tag{25}$$

At the same time, the sensitivity of this configuration against vibrations is much reduced because the differential phase of two

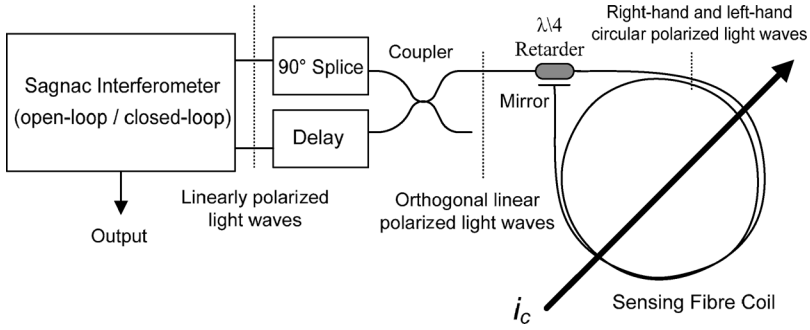

Fig. 38. Schematic of a reflective interferometer where left- and right-hand circular polarized light waves are feed into the coil at one end and reflected by a mirror at the other end. This technique has vastly improved immunity to vibrations and a doubling of the sensitivity over the original Sagnac method since the light effectively travels two times through the coil.

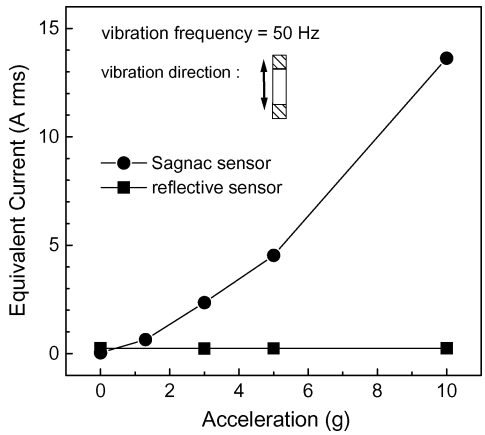

Fig. 39. Current errors generated via vibrations of the coils for Sagnac and reflective interferometers, showing the superior performance of the reflective interferometer over the classical Sagnac interferometer [70].

Fig. 40. Commercial available fiber-optic-current-sensors (FOCSs) capable of measuring several hundred kA (photo courtesy ABB, Inc.).

orthogonal light waves is around 1000 times less disturbed than the phase of the two independent light waves of the Sagnac interferometer (Fig. 39) [70]. A coupler, delay line and 90° splice is required to convert the orthogonal linear polarized light waves to two separate linear polarized light waves that can be processed by the Sagnac interferometer. The phase shift between the linear polarized light waves can be measured using a standard open-loop or closed-loop Sagnac interferometer method as discussed previously.

C. Conclusion for Faraday Effect-Based Current Sensors

In order to avoid stress on the fiber-optic cable, the cable is packaged so as to protect the cable from any stress due to mounting and transportation of the current sensor. The fiber-optic current sensor, nevertheless, allows a significant reduction in power consumption and bulk compared with alternative technologies that are used in power distribution systems (Fig. 40). For smaller current magnitudes, other principles are more attractive since they are less expensive, and the fiber-optic principle would require many turns to provide satisfactory sensitivity. Moreover, this would involve the use of a special and expensive fiber optical cable in order to avoid bending stress, which otherwise deteriorates the performance. Increased sensitivity can also be achieved by using experimentally available fiber optical cables with higher Verdet constant. However, these experimental cables only allow a gain in sensitivity of less than ten at the expense of an increased thermal drift. As pointed out before, fiber-optic current sensors are especially useful in high voltage systems because of the inherent electrical isolation, and in systems with high electromagnetic-inference levels. They are usually employed in power metering, fault detection and electrowinning applications.

VI. Conclusion

The performance of the different current sensing techniques is compared in Table II, with the costs and common applications given in Table III. Shunt resistors are widely used to measure currents on printed-circuit-boards due to their simplicity and reasonable accuracy. At higher currents, the shunt resistor becomes troublesome due to the high-power losses and the associated increase in size. An alternative is the copper trace sensing

TABLE II
PERFORMANCE COMPARISON

	Bandwidth	DC Capable	Accuracy	Thermal drift [ppm/K]	Isolated	Range	Power Loss
Shunt Resistor • Coaxial • SMD	MHz kHz-MHz	Yes	0.1% – 2%	25 – 300	No	kA mA – A	W – kW mW – W
Copper Trace[1]	kHz	Yes	0.5% – 5%	50 – 200	No	A – kA	mW
Current Transformer	kHz-MHz	No	0.1% – 1%	< 100	Yes	A – kA	mW
Rogowski Coil	kHz-MHz	No	0.2% – 5%	50 – 300	Yes	A – MA	mW
Hall Effect [1] (open-loop / closed-loop)	kHz	Yes	0.5% – 5%	50 – 1000	Yes	A – kA	mW
Fluxgate	kHz	Yes	0.001% – 0.5%	< 50	Yes	mA – kA	mW – W
AMR Effect[1] (closed-loop, core-less)	kHz	Yes	0.5% – 2%	100 – 200	Yes	A	mW
Core-less open-loop (GMR, AMR, Hall Effect)[1]	kHz	Yes	1% – 10%	200 – 1000	Yes	mA – kA	mW
Fiber-Optic Current Sensor[1]	kHz-MHz	Yes	0.1% – 1%	< 100	Yes	kA – MA	W

[1] Using temperature compensation electronics

TABLE III
APPLICATION HINTS

	Cost[3] [USD]	Size [mm^3]	Limitations
Shunt Resistor[1]	> 0.5	> 25	An overcurrent can permanently damage the shunt resistor. High power losses make it difficult to measure high currents. In high voltage applications the missing electrical isolation is a problem.
Copper Trace[1,2]	> 0.5	> 25	The accuracy is degraded by noise due to the high amplification. The bandwidth may be limited by the gain-bandwidth product of the amplifier. Measuring the trace temperature might be difficult in some applications. No electrical isolation.
Current Transformer	> 0.5	> 500	A DC offset may saturate core material. For high currents a large core cross sectional area is required to avoid saturation. In high voltage applications the winding isolation becomes crucial. A high winding ratio leads to increased parasitic capacitance, which reduces the measurement bandwidth and common mode noise rejection.
Rogowski Coil	> 1	> 1000	The accuracy depends on the conductor position. Difficult to measure small currents due to poor sensitivity. A high number of turns reduces the measurement bandwidth.
Hall Effect (open-loop / closed-loop)	> 4	> 1000	AC currents with high frequency can overheat the core material. An overcurrent incident does introduce a magnetic offset that can only be eliminated with a degaussing cycle. Distinct thermal drift that has to be compensated.
Fluxgate	> 10	> 1000	Some variants induce notable voltage noise into the primary winding. Complicated control electronics. A high number of turns reduces the measurement bandwidth.
AMR Effect (closed-loop, core-less)	> 5	> 1000	Not practical for very high currents since the current has to flow through the sensor housing. Susceptible to external magnetic stray fields. Bandwidth limited to <1 MHz.
Core-less open-loop (GMR, AMR, Hall Effect)	> 2	> 25	Highly susceptible to external magnetic fields. If the sensor is close to the current carrying conductor, the skin effect may limit the frequency response.
Fiber-Optic Current Sensor	> 1k	> 10^6	Due to high complexity not suitable to measure small currents. Bending stress of the fiber-optic cable deteriorates the accuracy.

[1] Including amplification.
[2] Including temperature sensor.
[3] In high volume applications.

approach, which provides low power losses and low cost. However, temperature sensors are required to compensate for the distinct thermal drift and the bandwidth is limited due to the use of high gain amplifiers, mutual inductance, and skin effect.

Hall-effect current sensors, on the other hand, provide an alternative with low losses, galvanic isolation, high bandwidth and good accuracy, but at a much higher price. These sensors are used in a wide range of different applications like automo-

tive, industrial, or energy distribution. Closed-loop AMR-based current sensors provide similar if not better performance than Hall-effect sensors but, so far, are only available for current ranges from one ampere up to over hundred amperes, and are more costly than Hall-effect sensors. For highest performance, fluxgate current sensors are used but due to their high price are suitable only for specialized applications. For very high direct currents, fiber-optic current sensors are state-of-the-art.

Current transformers and Rogowski coils are popular techniques for measuring alternating currents and are widely used in power electronics and energy distribution. These principles can be adapted to measure currents from amperes up to mega amperes providing high accuracy and galvanic isolation at relatively low cost.

Recently, numerous core-less and open-loop magnetic field sensing ICs based on Hall-effect, AMR, and GMR have become available that enable indirect current sensing at low bulk and reasonable price. However, the accuracy may be low due to the skin effect inside the primary conductor that causes a change in the magnetic field, and they are sensitive to external magnetic fields that are difficult to shield.

The high-cost pressure in the power electronics industry means that few options to shunt resistors are open to power electronics engineers. For high direct currents, the copper trace sense approach might be an alternative but sacrifices some accuracy and bandwidth. The current transformer can be an attractive choice if the current is chopped inside a switched mode power converter, and allows the transformer to demagnetize periodically in order to avoid saturation.

As is often the case the engineer will face a tradeoff between cost, bandwidth, power loss, and accuracy.

ACKNOWLEDGMENT

The authors would like to thank K. Bohnert from ABB Switzerland for its valuable information and comments on the fiber-optic current sensor.

REFERENCES

[1] F. W. Grover, *Inductance Calculations: Working Formulas and Tables*. New York: D. Van Nostrand, 1946.

[2] C. M. Johnson and P. R. Palmer, "Current measurement using compensated coaxial shunts," *Proc. IEE Sci., Measure. Technol.*, vol. 141, pp. 471–480, 1994.

[3] J. A. Ferreira, W. A. Cronje, and W. A. Relihan, "Integration of high frequency current shunts in power electronic circuits," *IEEE Trans. Power Electron.*, vol. 10, pp. 32–37, 1995.

[4] R. Malewski, "New device for current measurement in exploding wire circuits," *Rev. Scient. Instruments*, vol. 39, pp. 90–94, 1968.

[5] R. Malewski, C. T. Nguyen, K. Feser, and N. Hylten-Cavallius, "Elimination of the skin effect error in heavy-current shunts," *IEEE Trans. Power Apparatus and Systems*, vol. PAS-100, pp. 1333–1340, 1981.

[6] F. Castelli, "The flat strap sandwich shunt," *IEEE Trans. Instrument. Measure.*, vol. 48, pp. 894–898, 1999.

[7] F. Costa, P. Poulichet, F. Mazaleyrat, and E. Labouré, "The current sensors in power electronics, a review," *EPE Journal*, vol. 11, pp. 7–18, 2001.

[8] E. Dallago, M. Passoni, and G. Sassone, "Lossless current sensing in low-voltage high-current DC/DC modular supplies," *IEEE Trans. Ind. Electron.*, vol. 47, pp. 1249–1252, 2000.

[9] B. Mammano, "Current sensing solutions for power supply designer," in *Power Design Seminar SEM 1200*, 1997, Unitrode Corp..

[10] B. Mammano, High-side current-sense measurement, Appl. Rep. AN 746, Maxim Integrated Products, Inc., 2005.

[11] L. Spaziani, Using copper PCB etch for low value resistance Texas Instruments, Appl. Rep. DN-71, 1997.

[12] L. Spaziani, Cu-ETP copper specification, German Copper Institute., 2005. [Online]. Available: http://www.kupfer-institut.de/front_frame/pdf/Cu-ETP.pdf, 2005

[13] S. Ziegler, H. H. C. Iu, R. C. Woodward, and L. J. Borle, "Theoretical and practical analysis of a current sensing principle that exploits the resistance of the copper trace," in *Proc. 39th IEEE Power Electronics Specialists Conf., PESC'08*, Rhodes, Greece, 2008, pp. 4790–4796.

[14] S. Ziegler, R. C. Woodward, H. H. C. Iu, and L. J. Borle, "Investigation into static and dynamic performance of the copper trace current sense method," *IEEE Sensors J.*, 2009, accepted for publication.

[15] G. Eirea and S. R. Sanders, "High precision load current sensing using on-line calibration of trace resistance," *IEEE Trans. Power Electron.*, vol. 23, pp. 907–914, 2008.

[16] W. F. Ray and C. R. Hewson, "High performance Rogowski current transducers," in *Proc. IEEE Ind. Appl. Conf.*, Rome, Italy, 2000, pp. 3083–3090.

[17] W. F. Ray and C. R. Hewson, RCTrms Rogowski coil datasheet Power Electronic Measurements Ltd., 2005. [Online]. Available: http://www.pemuk.com

[18] D. A. Ward and J. L. T. Exon, "Using Rogowski coils for transient current measurements," *Eng. Sci. Education J.*, vol. 2, pp. 105–113, 1993.

[19] A. Radun, "An alternative low-cost current-sensing scheme for high-current power electronics circuits," *IEEE Trans. Ind. Electron.*, vol. 42, pp. 78–84, 1995.

[20] L. Dalessandro, N. Karrer, M. Ciappaz, A. Castellazzi, and W. Fichtner, "Online and offline isolated current monitoring of parallel switched high-voltage multi-chip IGBT modules," in *Proc. 39th IEEE Power Electron. Specialists Conf., PESC'08*, Rhodes, Greece, 2008, pp. 2600–2606.

[21] L. Zhao, J. D. v. Wyk, and W. G. Odendaal, "Planar embedded pick-up coil sensor for integrated power electronic modules," in *Proc. Appl. Power Electron. Conf. Expo., APEC*, Anaheim, CA, 2004, vol. 2, pp. 945–951.

[22] J. P. Dupraz, A. Fanget, W. Grieshaber, and G. F. Montillet, "Rogowski coil: Exceptional current measurement tool for almost any application," in *Proc. IEEE Power Eng. Soc. General Meeting*, Tampa, FL, 2007, pp. 1–8.

[23] N. McNeill, N. K. Gupta, S. G. Burrow, D. Holliday, and P. H. Mellor, "Application of reset voltage feedback for droop minimization in the unidirectional current pulse transformer," *IEEE Trans. Power Electron.*, vol. 23, pp. 591–599, 2008.

[24] N. McNeill, N. K. Gupta, and W. G. Armstrong, "Active current transformer circuits for low distortion sensing in switched mode power converters," *IEEE Trans. Power Electron.*, vol. 19, pp. 908–917, 2004.

[25] K.-w. Ma and Y.-s. Lee, "Technique for sensing inductor and DC output currents of PWM DC-DC converter," *IEEE Trans. Power Electron.*, vol. 9, pp. 346–354, 1994.

[26] K.-w. Ma and Y.-s. Lee, Isolated Current and Voltage Transducers Appl. Rep., LEM, 2004.

[27] L. Dalessandro, N. Karrer, and J. W. Kolar, "High-performance planar isolated current sensor for power electronics applications," *IEEE Trans. Power Electron.*, vol. 22, pp. 1682–1691, 2007.

[28] P. Poulichet, F. Costa, and É. Labouré, "A new high-current large-bandwidth dc active current probe for power electronics measurements," *IEEE Trans. Ind. Electron.*, vol. 52, pp. 243–254, 2005.

[29] P. A. Tipler, *Physics for Scientists and Engineers*. New York: Worth Publishers, Inc., 1991.

[30] P. A. Tipler, An introduction to the Hall effect, Bell Technologies, Inc., 2005. [Online]. Available: http://www.fwbell.com

[31] P. A. Tipler, Understanding Hall effect devices, Bell Technologies, Inc., 2005. [Online]. Available: http://www.fwbell.com

[32] R. S. Popovic, Z. Randjelovic, and D. Manic, "Integrated Hall-effect magnetic sensors," *Sens. Actuators A: Physical*, vol. 91, pp. 46–50, 2001.

[33] J. Lenz and A. S. Edelstein, "Magnetic sensors and their applications," *IEEE Sensors J.*, vol. 6, pp. 631–649, 2006.

[34] P. Ripka, "Review of fluxgate sensors," *Sens. Actuators A: Physical*, vol. 33, pp. 129–141, 1992.

[35] F. Primdahl, "The fluxgate magnetometer," *J. Physics E: Scientific Instruments*, vol. 12, pp. 241–253, 1979.

[36] P. Ripka, "Advances in fluxgate sensors," *Sens. Actuators A: Physical*, vol. 106, pp. 8–14, 2003.

[37] F. Primdahl, "The fluxgate mechanism, part I: The gating curves of parallel and orthogonal fluxgates," *IEEE Trans. Magn.*, vol. 6, pp. 376–383, 1970.
[38] S. Ziegler, P. Gammenthaler, and A. Chapuis, An isolated current to voltage, voltage to voltage converter U. S. P. T. Office, Ed., USA, Power-One, Inc., 2008, (Application filed).
[39] S. Ziegler, L. Borle, and H. H. C. Iu, "Transformer based DC current sensor for digitally controlled power supplies," in *Proc. Australasian Universities Power Eng. Conf. 2007*, Perth, Australia, 2007, pp. 525–530.
[40] M. Román, G. Velasco, A. Conesa, and F. Jeréz, "Low consumption fluxgate transducer for AC and DC high-current measurement," in *Proc. 39th IEEE Power Electron. Specialists Conf., PESC'08*, Rhodes, Greece, 2008, pp. 535–560.
[41] P. Pejovic, "A simple circuit for direct current measurement using a transformer," *IEEE Trans. Circuits, Syst,-I: Fundamental Theory and Applications*, vol. 45, pp. 830–837, 1998.
[42] I. M. Filanovsky and V. A. Piskarev, "Sensing and measurement of DC current using a transformer and RL-multivibrator," *IEEE Trans. Circuits, Syst.*, vol. 38, pp. 1366–1370, 1991.
[43] K. Harda and H. Sakamoto, "Current sensors with a small saturable core and MOSFETs," *IEEE Trans. Magn.*, vol. 24, pp. 2910–2912, 1988.
[44] P. Ripka, J. Kubik, M. Duffy, W. G. Hurley, and S. O'Reilly, "Current sensor in PCB technology," *IEEE Sensors J.*, vol. 5, pp. 433–438, 2005.
[45] O. Dezuari, E. Belloy, S. E. Gilbert, and M. A. M. Gijs, "Printed circuit board integrated fluxgate sensor," *Sens. Actuators A: Physical*, vol. 81, pp. 200–203, 2000.
[46] O. Dezuari, E. Belloy, S. E. Gilbert, and M. A. M. Gijs, Basic introduction to the use of magnetoresistive sensors, Appl. Rep. AN 37, Zetex Semiconductors, Inc., 2003.
[47] G. Laimer and J. W. Kolar, "Design and experimental analysis of a DC to 1 MHz closed loop magnetoresistive current sensor," in *Proc. Appl. Power Electron. Conf. Exposition, APEC'05*, Austin, TX, 2005, vol. 2, pp. 1288–1292.
[48] G. Binasch, P. Grünberg, F. Saurenbach, and W. Zinn, "Enhanced magnetoresistance in layered magnetic structures with antiferromagnetic interlayer exchange," *Phys. Rev. B*, vol. 39, pp. 4828–4830, 1989.
[49] M. N. Baibich, J. M. Broto, A. Fert, F. N. V. Dau, F. Petroff, P. Eitenne, G. Creuzet, A. Friederich, and J. Chazelas, "Giant magnetoresistance of (001)Fe/(001)Cr magnetic superlattices," *Phys. Rev. Lett.*, vol. 61, pp. 2472–2475, 1988.
[50] M. N. Baibich, J. M. Broto, A. Fert, F. N. V. Dau, F. Petroff, P. Eitenne, G. Creuzet, A. Friederich, and J. Chazelas, The giant magnetoresistive head: A giant leap for IBM research IBM Research, 1997. [Online]. Available: http://www.research.ibm.com/research/gmr.html
[51] K.-M. H. Lenssen, D. J. Adelerhof, H. J. Gassen, A. E. T. Kuiper, G. H. J. Somers, and J. B. A. D. v. Zon, "Robust giant magnetoresistance sensors," *Sens. Actuators A: Physical*, vol. 85, pp. 1–8, 2000.
[52] C. Reig, D. Ramirez, F. Silva, J. Bernardo, and P. Freitas, "Design, fabrication, and analysis of a spin-valve based current sensor," *Sens. Actuators A: Physical*, vol. 115, pp. 259–266, 2004.
[53] H. Beltran, C. Reig, V. Fuster, D. Ramírez, and M. D. Cubells-Beltrán, "Modeling of magnetoresistive-based electrical current sensors: A technological approach," *IEEE Sensors J.*, vol. 7, pp. 1532–1537, 2007.
[54] H. Beltran, C. Reig, V. Fuster, D. Ramírez, and M. D. Cubells-Beltrán, AA and AB-series analog sensors datasheet NVE, Inc., 2005. [Online]. Available: http://www.nve.com
[55] I. Jedlicska, R. Weiss, and R. Weigel, "Improving GMR current sensor measurements through hysteresis modeling," in *Proc. 39th IEEE Power Electron. Specialists Conf., PESC'08*, Rhodes, Greece, 2008, pp. 4781–4785.
[56] P. Kowina, H. Reeg, A. Peters, M. Haepe, W.-J. Becker, and W. Ricken, "High dynamic magnetic beam current measurement by means of optimized magnet-resistance (MR) sensor engineering," in *Proc. 7th Eur. Workshop on Beam Diagnostics and Instrumentation for Particle Accelerators, DIPAC 2005*, Lyon, 2005, pp. 102–104.
[57] X. P. Li, Z. J. Zhao, C. Chua, H. L. Seet, and L. Lu, "Enhancement of giant magnetoimpedance effect of electroplated NiFe/Cu composite wires by dc Joule annealing," *J. Appl. Phys.*, vol. 94, pp. 7626–7630, 2003.
[58] R. S. Beach and A. E. Berkowitz, "Giant magnetic field dependent impedance of amorphous FeCoSiB wire," *Appl. Phys. Lett.*, vol. 64, pp. 3652–3654, 1994.
[59] T. Miyazaki and N. Tezuka, "Giant magnetic tunneling effect in Fe/Al2O3/Fe junction," *J. Magn. Magn. Mater.*, vol. 139, pp. 231–234, 1994.
[60] D. D. Djayaprawira, K. Tsunekawa, M. Nagai, H. Maehara, S. Yamagata, N. Watanabe, S. Yuasa, Y. Suzuki, and K. Ando, "230% room-temperature magnetoresistance in CoFeB/MgO/CoFeB magnetic tunnel junctions," *Appl. Phys. Lett.*, vol. 86, p. 092502, 2005.
[61] E. Udd*, Fiber Optic Sensors—An Introduction for Engineers and Scientists*. New York: Wiley, 1991.
[62] B. Lee, "Review of the present status of optical fiber sensors," *Opt. Fiber Technol.*, vol. 9, pp. 57–79, 2003.
[63] K. Bohnert, P. Gabus, J. Nehring, H. Brändle, and M. G. Brunzel, "Fiber-optic current sensor for electrowinning of metals," *J. Lightwave Technol.*, vol. 25, pp. 1–8, 2007.
[64] K. Bohnert, H. Brändle, M. G. Brunzel, P. Gabus, and P. Guggenbach, "Highly accurate fiber-optic DC current sensor for the electrowinning Industry," *IEEE Trans. Ind. Appl.*, vol. 43, pp. 180–187, 2007.
[65] A. Papp and H. Harms, "Magnetooptical current transformer 1: Principles," *Appl. Opt.*, vol. 19, pp. 3729–3734, 1980.
[66] T. W. Cease and P. Johnston, "A magneto-optic current transducer," *IEEE Trans. Power Delivery*, vol. 5, pp. 548–555, 1990.
[67] P. A. Nicati and P. Robert, "Stabilized current sensor using a Sagnac interferometer," *J. Phys. E: Sci. Instrum.*, vol. 21, pp. 791–796, 1988.
[68] A. J. Rogers, J. Xu, and J. Yao, "Vibration immunity for optical-fiber current measurement," *J. Lightwave Technol.*, vol. 13, pp. 1371–1377, 1995.
[69] M. J. Blake, P. Tantaswadi, and R. T. d. Carvalho, "In-line Sagnac interferometer current sensor," *IEEE Trans. Power Delivery*, vol. 11, pp. 116–121, 1996.
[70] K. Bohnert, P. Gabus, J. Nehring, and H. Brändle, "Temperature and vibration insensitive fiber-optic current sensor," *J. Lightwave Technol.*, vol. 20, pp. 267–276, 2002.
[71] A. H. Rose, S. M. Etzel, and C. M. Wang, "Verdet constant dispersion in annealed optical fiber current sensors," *J. Lightwave Technol.*, vol. 15, pp. 803–807, 1997.
[72] S. X. Short, P. Tantaswadi, R. T. de Carvalho, B. D. Russell, and J. Blake, "An experimental study of acoustic vibration effects in optical fiber current sensors," *IEEE Trans. Power Delivery*, vol. 11, pp. 1702–1706, 1996.
[73] G. Frosio and R. Dändliker, "Reciprocal reflection interferometer for a fiber-optic Faraday current sensor," *Appl. Opt.*, vol. 33, pp. 6111–6122, 1994.

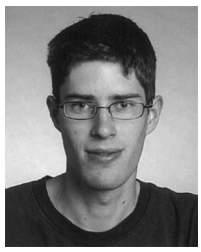

Silvio Ziegler received the B.Eng. degree in electrical engineering from Bern University of Applied Sciences, Bern, Switzerland, in 2006. He is currently working towards the Ph.D. degree in electrical and electronics engineering at the University of Western Australia, Crawley, Australia.

In 2006 he was with Bachmann Electronic, Feldkirch, Austria, working as a Digital Design Engineer. His research interests include current sensing techniques, switched mode power converters, and digital control techniques.

Robert C. Woodward received the B.Appl.Sc. degree in metallurgy from Curtin University, Perth, Australia, in 1987 and the Ph.D. degree in magnetization mechanisms in rare earth-based permanent magnets at the from University of Western Australia, Crawley, Australia, in 2003.

He is presently a Research Fellow in the Centre for Strategic Nanofabrication within the School of Physics, University of Western Australia.

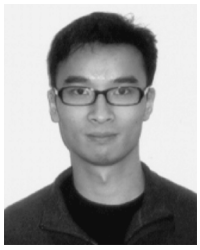

Herbert Ho-Ching Iu (S'98–M'00–SM'06) received the B.Eng. (Hons) degree in electrical and electronics engineering from the University of Hong Kong, Hong Kong, in 1997 and the PhD. degree from the Hong Kong Polytechnic University, Hong Kong, in 2000.

In 2002, he joined the School of Electrical, Electronic and Computer Engineering, University of Western Australia as a Lecturer. He is currently an Associate Professor at the University of Western Australia. He has published over 90 papers in these areas. He served as a Visiting Lecturer at the University of Reims Champagne-Ardenne, France, in 2004, and a Visiting Assistant Professor at the Hong Kong Polytechnic University, Hong Kong, in 2006. He currently serves as an Editorial Board Member for the *Australian Journal of Electrical and Electronics Engineering*, a Guest Editor for *Circuits, Systems and Signal Processing*, and an Associate Editor for IEEE *Circuits and Systems Society Newsletter*. He is a Co-Editor of Control of Chaos in Nonlinear Circuits and Systems (Singapore: World Scientific, 2009). His research interests include power electronics, renewable energy, nonlinear dynamics, current sensing techniques, TCP dynamics, and computational intelligence.

Lawrence J. Borle (S'79–M'85) received the B.Sc. and M.Sc. degrees from the University of Alberta, Edmonton, AB, Canada, in 1982 and 1991, respectively, both in electrical engineering, and the Ph.D degree in electrical engineering (power electronics) from Curtin University of Technology, Perth, Australia in 2000.

From 1982 to 1985, he was with Chevron Canada Resources Ltd., Calgary, Canada, doing electrical and instrumentation engineering work, and having responsibility for company radio systems engineering. From 1985 to 1988, he worked for Nova Corporation of Alberta, Edmonton, doing electrical and instrumentation engineering work. He returned to University in 1988, studying power electronics. After receiving the M.Sc. degree in 1991, he worked as a Research Fellow on current-controlled grid-connected inverters in joint venture projects between Curtin University of Technology (CUT) and Advanced Energy Systems Pty. Ltd. (AES), both in Perth, Western Australia. From 1994 to 2000, he was with PowerSearch, Ltd., the research and development group of AES, and was leading the commercialization of current-controlled inverters. In 2000, he became a Lecturer (power electronics) at CUT, and then was a Senior Lecturer in the School of Electrical, Electronic and Computer Engineering, University of Western Australia from 2002 to 2007. Since 2007, he has been working as a Senior Engineer and R&D Leader with SunEnergy Limited, Perth.

Dr. Borle is a Chartered Professional Engineer of the Institution of Engineers, Australia, and is registered on Section Three of the National Professional Engineers Register (NPER-3). He is also a member of the Association of Professional Engineers, Scientists and Managers, Australia.